Magnetic and Transport Properties of $(Ba_{1-x}K_x)Fe_2As_2$

by

Patrick Reuvekamp

B.Sc., Brock University, 2006

A THESIS SUBMITTED IN PARTIAL FULFILMENT OF
THE REQUIREMENTS FOR THE DEGREE OF

MASTER OF SCIENCE

in

The Faculty of Mathematics and Sciences

Department of Physics

BROCK UNIVERSITY

August 17, 2009

In presenting this thesis in partial fulfilment of the requirements for an advanced degree at Brock University, I agree that the Library shall make it freely available for reference and study. I further agree that permission for extensive copying of this thesis for scholarly purposes may be granted by the head of my department or by his or her representatives. It is understood that copying or publication of this thesis for financial gain shall not be allowed without my written permission.

(Signature) _____

Department of Physics

Brock University
St.Catharines, Canada

Date _____

Abstract

Single crystals of $(Ba_{1-x}K_x)Fe_2As_2$ were prepared using the Sn flux method. Two heating methods were used to prepare the single crystals: the slow heating and rapid heating methods. It was found that the single crystals grown using the slow heating method were not superconducting due to a significant loss of potassium. When the rapid heating method was used, the single crystals were observed to be superconducting with the desired potassium concentration. The energy dispersive X-ray spectroscopy analysis indicated the presence of multiple phases in the single crystals. Using single crystal X-ray diffraction, the crystal structure of the single crystals was found to be I4/mmm tetragonal at room temperature. The magnetic measurements on the single crystals indicated the presence of multiple phases and magnetic impurities.

Contents

List of Tables

List of Figures

Preface

P. Reuvekamp and F. S. Razavi and C. Hoch and J. S. Kim and R. K. Kremer and A. Simon. Spontaneous Stoichiometry Change in Single Crystals of Superconducting $(Ba_{1-x}K_x)Fe_2As_2$ Grown by a Rapid-Heating Sn-Flux Method. *J. Supercond. Nov. Magn.*, 22: 353 – 356.

Acknowledgements

Over the last two years, there have been many people who have contributed to my research work and education. Firstly, I would like to thank my supervisor and mentor, Dr. F.S. Razavi, for his understanding and infinite patience. I would like to thank Dr. R.K. Kremer, Dr. J.S. Kim, Dr. C. Hoch, Frau Brücher, Frau Siegle, and Herr Höhn of Chemieservice at the Max-Planck-Institut für Festkörperforschung for their experimental assistance during the preparation and the measurements of the single crystals. I would like to thank the faculty of the Physics department for their guidance and assistance, particularly Dr. M. Reedyk for proof-reading this thesis. Furthermore, I would like to thank my friends in the Physics department and elsewhere in Brock who where always helpful and understanding. I would particularly like to thank my parents for supporting me through my education and the many challenges along the way.

Chapter 1

Introduction

$(Ba_{1-x}K_x)Fe_2As_2$ belongs to the more general family of compounds called Iron Arsenic superconductors. Currently, there exists four similar classes of compounds: RFeAsO where R = La or Sm [1, 2], AFe_2As_2 where A = Ca, Ba, Sr or Eu[3–8], LiFeAs [9–11] and SrFeAsF [12, 13]. The first superconductor to be found in this general family was LaPOFe (T_c = 5 K) by Kamihara *et al.*[14] in 2006. But it was not until La(O/F)FeAs (T_c = 26 K[1] and 43 K at 4 GPa[2]) was discovered by Kamihara *et al.*[1, 2] that researchers focused on the compounds with iron arsenic planes. Quickly after the discovery of La(O/F)FeAs, Sm(O/F)FeAs was synthesized by Ren *et al.*[15]. Moreover, Sm(O/F)FeAs has the highest T_c of any compound in the above four groups with a T_c of 55 K. Hence this family of compounds represents a second class of High T_c superconductors due to their high superconducting transition temperatures[16]. Furthermore, $(Ba_{1-x}K_x)Fe_2As_2$ superconductors have the highest known T_c of the AFe_2As_2 compounds[17] and also when compared with compounds with the same crystal structure (tetragonal I4/mmm) where the highest T_c reached was 26 K for the borocarbide YPd_2B_2C[18, 19].

After the discovery of La(O/F)FeAs compounds, researchers shifted their focus to finding similar compounds. Rotter *et al.*[3] proposed that $BaFe_2As_2$ could be doped to become a superconductor due to the presence of iron arsenic layers as well as having the same charge and similar magnetic and electric properties as La(O/F)FeAs. When lanthanum was chosen as the first doping element, only the antiferromagnetic

transition was suppressed but no superconductivity was observed[3, 20]. Instead potassium was used to create a hole-doped superconductor with a T_c of 38.1 K[3]. A week later, Wang *et al.*[4] and Ni *et al.*[5] created single crystals of $(Ba_{1-x}K_x)Fe_2As_2$ using the flux methods[3–5] .

1.1 Crystal Structure of $(Ba_{1-x}K_x)Fe_2As_2$

The ternary parent compound, $BaFe_2As_2$, has a body centered tetragonal structure at 300 K belonging to the $ThCr_2Si_2$ structure with space group 139 – I4/mmm[18], as seen in Figure 1.1. Barium sites are located on the four corners of the top and bottom and one at the body center while the iron and arsenic forms sheets located above and below the body center barium site[18]. The two iron arsenic sheets consist of edge-sharing $FeAs_4$ tetrahedra with a mirror plane located at the center barium site[17, 21]. A structural phase (orthorhombic distortion) transition occurs at 85 K and 140 K for Sn flux (see Figure 1.2) and polycrystalline/self flux samples (see Figure 1.3), respectively[17, 18]. The structural phase transition transforms the crystal structure from tetragonal I4/mmm to orthorhombic Fmmm. For example in polycrystalline $BaFe_2As_2$, the **a** and **b** axes are expanded from equality with a value of 3.9625 Å at 300 K to 5.6146 Å and 5.5742 Å respectively in the orthorhombic structure at 20K. The **c** axis decreases from 13.01 Å in the tetragonal phase at 300 K to 12.94 Å in the orthorhombic phase at 20 K[18]. The reduction of the structural phase transition temperature for Sn flux samples may be caused by the inclusion of Sn in the crystal structure but the exact mechanism remains unclear.

KFe_2As_2 also has tetragonal I4/mmm crystal structure albeit the lattice parameters change to 3.8414 Å and 13.839 Å for **a** and **c** respectively. KFe_2As_2 has a large **c**/**a** ratio and exhibits no orthorhombic distortion transition[8]. With the addition of

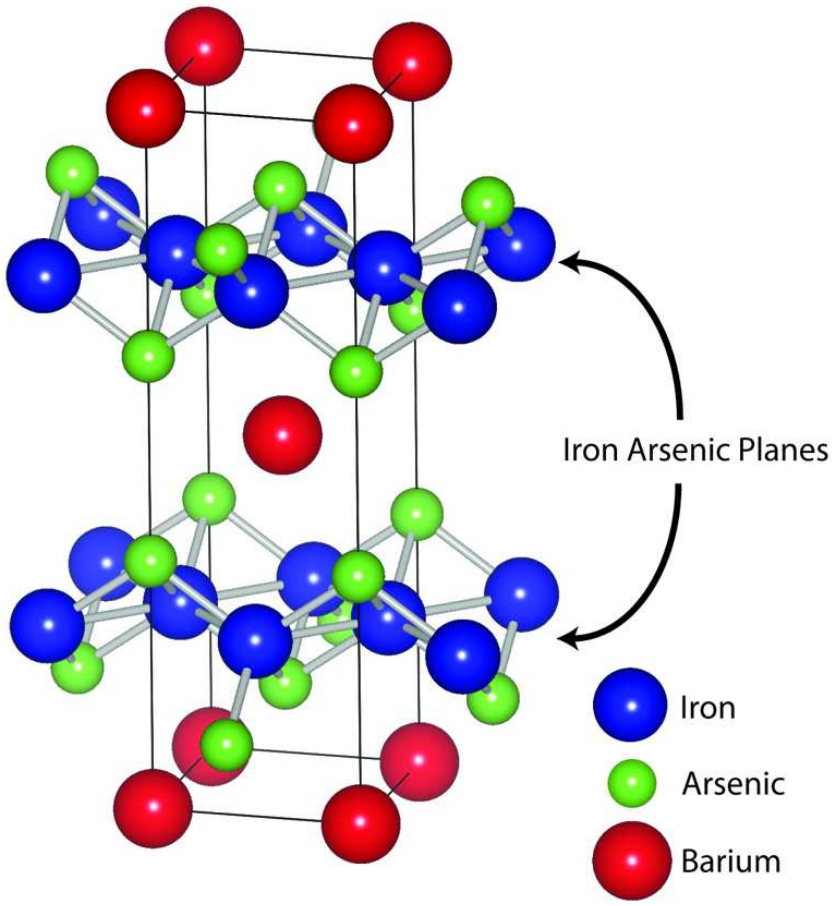

Figure 1.1: The tetragonal (I4/mmm) crystal structure of $BaFe_2As_2$ with barium sites in red, iron sites in blue and arsenic sites in green. This figure was prepared using Vesta software.

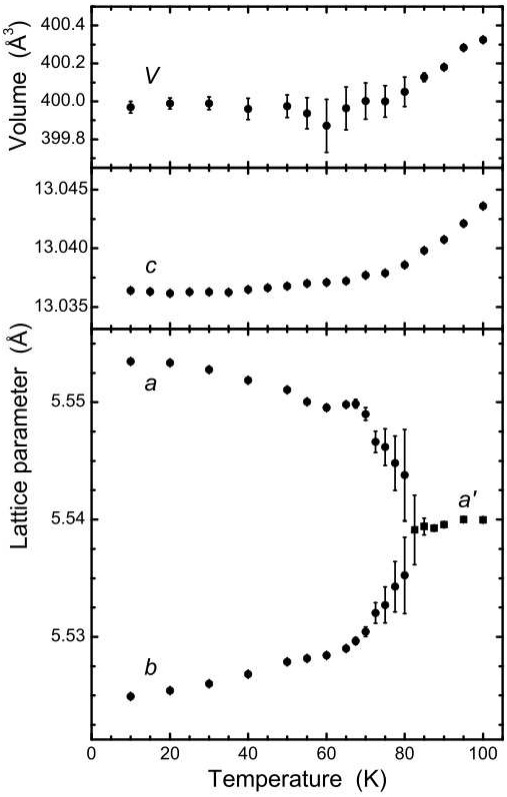

Figure 1.2: Lattice parameters and volume of the unit cell for a Sn flux $BaFe_2As_2$ single crystal at low temperature. **N.B.** $\mathbf{a}' = \sqrt{2}\mathbf{a}$. Reprinted from [5].

potassium to $BaFe_2As_2$, the lattice parameter **a** decreases to a minimum of 3.84 Å for $x = 1.0$ while the parameter **c** increases to maximum of 13.84 Å for $x = 1.0$. Furthermore, the Fe-Fe bond length and the bond angle ε of the As-Fe-As bond decreases monotonically as x increases, as seen in Figure 1.4. When $x = 0.2$ – 0.3, it was observed that the orthorhombic phase disappears and the crystal structure remains tetragonal I4/mmm[21], as seen in Figure 1.5 and 1.6. The loss of the orthorhombic distortion transition can be seen in Figure 1.6, where the splitting of the lattice parameters is absent for $x = 0.3$[17]. The exact placement and overall order of the barium and the potassium sites in the crystal structure is however still unclear.

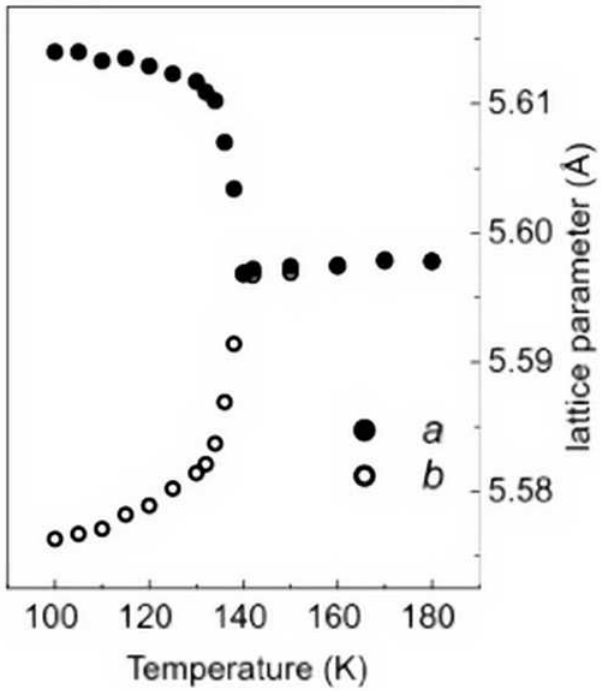

Figure 1.3: Lattice parameters for polycrystalline $BaFe_2As_2$ at low temperature. **N.B.** tetragonal **a** was multiplied by $\sqrt{2}$. Reprinted from [18].

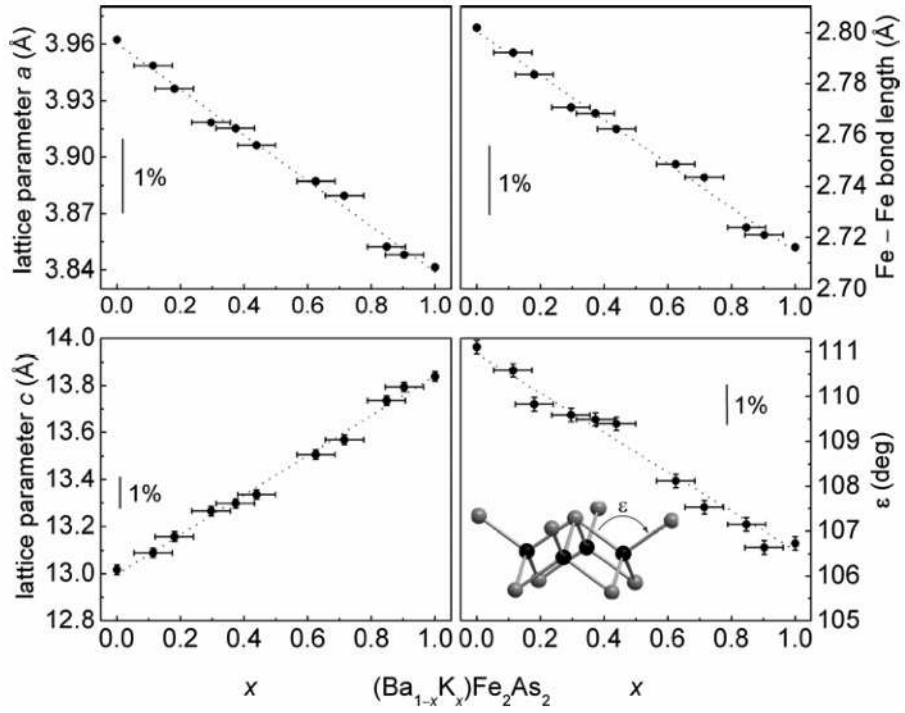

Figure 1.4: Effect of potassium doping (x) on the lattice parameters, angles, and bond lengths of $(Ba_{1-x}K_x)Fe_2As_2$ with $x = 0$ – 1. Reprinted from [17].

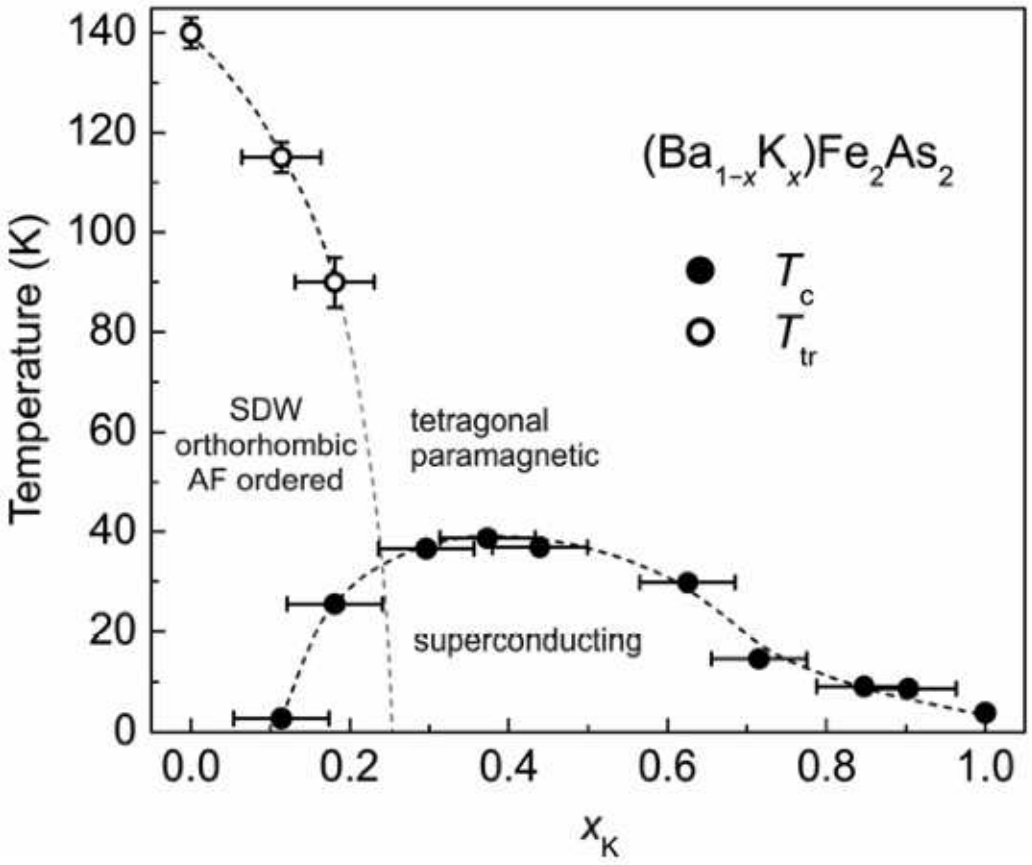

Figure 1.5: Structural phases, superconducting transition temperature (T_c), and structural transition temperature (T_{tr}) for $(Ba_{1-x}K_x)Fe_2As_2$ with $x = 0 - 1$. Reprinted from [17].

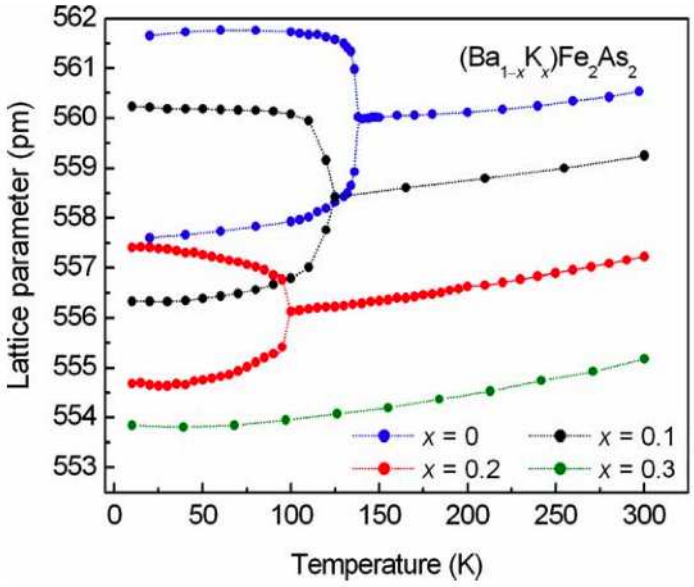

Figure 1.6: The variation in the lattice parameters of $(Ba_{1-x}K_x)Fe_2As_2$ for $x = 0$ – 0.3 where each left most top and bottom curves corresponds to the lattice parameters **a** and **b**, respectively. Reprinted from [17].

1.2 Magnetic Properties of $(Ba_{1-x}K_x)Fe_2As_2$

The parent compound, $BaFe_2As_2$, is a paramagnetic metal with a coupled structural and magnetic transition. The coupled structural and magnetic transitions causes the crystal structure to become orthorhombic (Fmmm) and a spin density wave (SDW) is observed[3, 18].

1.2.1 Paramagnetism

For $BaFe_2As_2$, the temperature dependent magnetic susceptibility varies depending on the method used to produce the sample. Rotter *et al.*[18] observed that polycrystalline $BaFe_2As_2$ (see Figure 1.7) is paramagnetic up to 140 K followed by an abrupt drop in susceptibility[18]. Ni *et al.*[5] used the Sn Flux method to create single crystals of $BaFe_2As_2$ and observed paramagnetism from 5 K to 300 K[5]. Wang *et al.*[4] used the self flux (FeAs) method to create single crystals of $BaFe_2As_2$ and observed Pauli paramagnetism up to 136 K followed by an abrupt drop in susceptibility due to the SDW transition[4]. The magnetic susceptibility curves for both flux methods can be seen in Figure 1.8. Su *et al.*[23] observed around 5% Sn in their Sn flux single crystals using Energy Dispersive X-ray spectroscopy (EDS) and furthermore their neutron diffraction data showed the presence of Sn[23]. Sun *et al.*[22] proposed that the Sn used in the flux replaces Fe sites in the crystal structure due to the similar ionic radii[22].

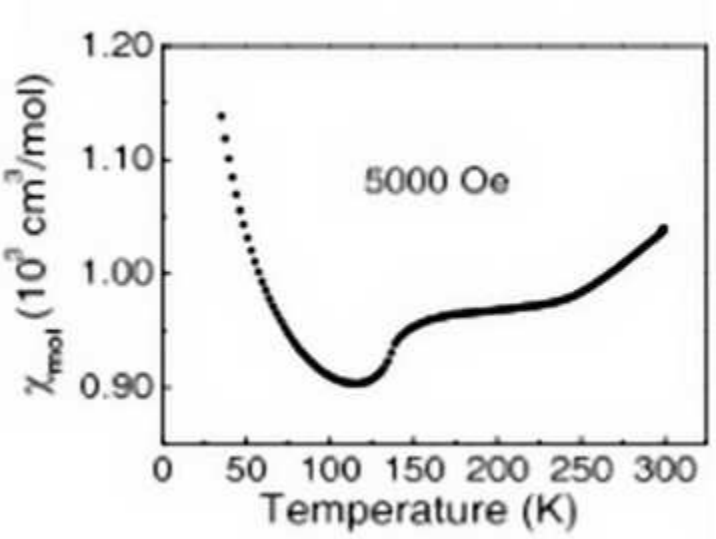

Figure 1.7: Magnetic susceptibility for polycrystalline $BaFe_2As_2$ where $H = 5000$ G. The increase in the susceptibility below 100 K was attributed to ferromagnetic impurities. Reprinted from [18].

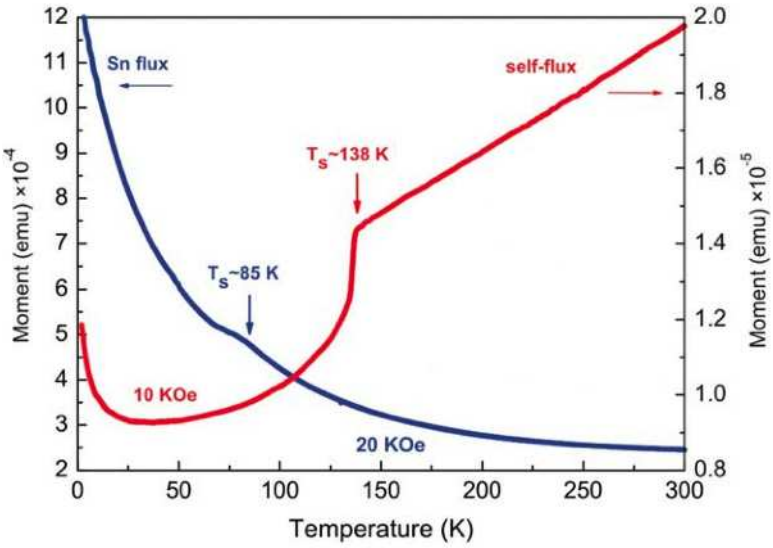

Figure 1.8: Magnetic susceptibility curves for Sn flux and self flux $BaFe_2As_2$ where the red curves represents self flux method and the blue curves represents the Sn flux method. Reprinted from [22].

1.2.2 Spin Density Wave and Antiferromagnetic Order

An interesting aspect in non-superconducting AFe_2As_2 compounds is the presence of a magnetic transition between 140 K and 200 K[8, 15, 18, 24]. In a similar compound, Dong *et al.*[25] proposed that the magnetic transition in La(O/F)FeAs is caused by a Spin Density Wave (SDW)[1] transition due to the strong nesting of the Fermi surface[2] with commensurate SDW vector[3] $\mathbf{Q}=(\pi,\pi,0)$[25]. Using neutron diffraction measurements, Huang *et al.*[26] observed that Nesting of the Fermi surface with $\mathbf{Q}=(\pi,\pi,0)$ and a SDW was also present in $BaFe_2As_2$ [26].

A common feature of non-superconducting AFe_2As_2 compounds is the coupling of the orthorhombic distortion and SDW transitions, see Table 1.1. In polycrystalline/self flux $BaFe_2As_2$, the coupled transition occurs at 140 K with the orthorhombic distortion of the crystal lattice and antiferromagnetic ordering[17]. The orthorhombic distortion of the crystal lattice causes the crystal structure to transform from tetragonal to orthorhombic while the SDW transition results in formation of antiferromagnetic order causing the moment of the iron atoms to become parallel with the longer **a** axis in the orthorhombic phase[17, 23, 26]. The magnetic structure of the $BaFe_2As_2$ can be seen in Figure 1.9. In polycrystalline/self flux $BaFe_2As_2$, the magnetic susceptibilities (see Figures 1.7 and 1.8) displays a clear and abrupt change near

[1] A Spin Density Wave (SDW) occurs when the spin of the electrons have a spatial oscillation with wavelength of $\lambda = \frac{2\pi}{\|\mathbf{Q}\|}$. The SDW state has a lower ground state energy than the Fermi sea resulting in the formation of an energy gap at the Fermi surface. See the references in Appendix A for more details on spin density waves.

[2] Nesting of the Fermi surface occurs when the surfaces of two different energy bands are connected by a vector **Q** (SDW vector). See the references in Appendix A for more details on the nesting of the Fermi surface.

[3] Commensurate SDW vector occur when the SDW vector has the same periodicity as the crystal lattice. See the references in Appendix A for more details on commensurate SDW.

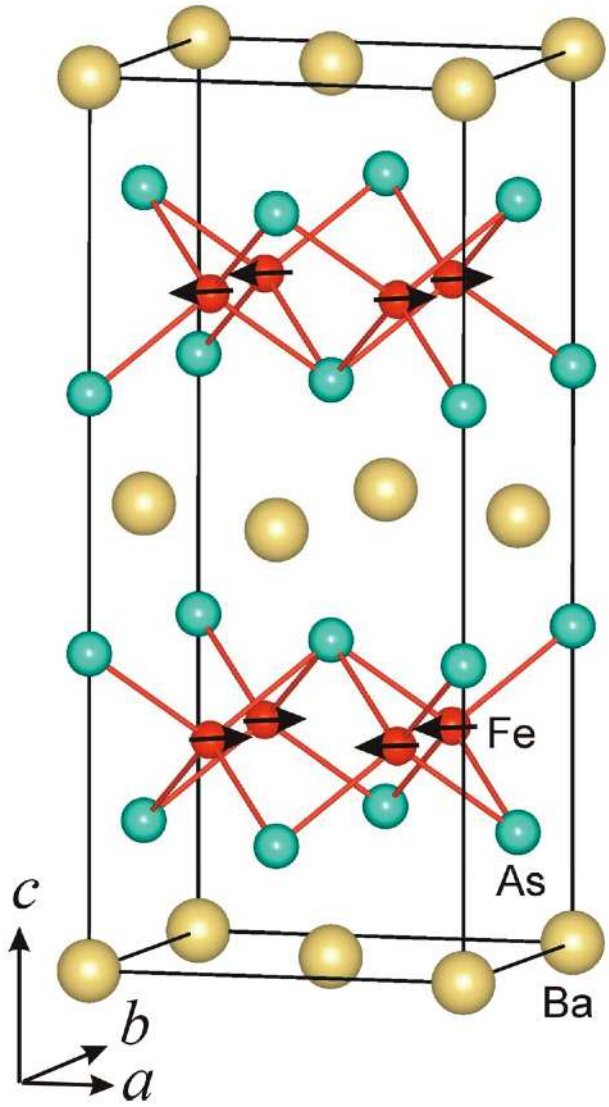

Figure 1.9: Magnetic structure of $BaFe_2As_2$ in the orthorhombic (Fmmm) crystal structure showing the alignment of the iron atom moments. Reprinted from [23].

Table 1.1: The coupled transition temperatures for the non-superconducting AFe_2As_2 compounds

Compound	T_{SDW}	Reference
$BaFe_2As_2$	140 K	Rotter *et al.*[18]
$CaFe_2As_2$	171 K	Ronning *et al.*[7]
$EuFe_2As_2$	190 K	Anupam *et al.*[6]
$SrFe_2As_2$	200 K	Sasmal *et al.*[8]

140 K[4, 18]. The abrupt change in the magnetic susceptibility of polycrystalline/self flux $BaFe_2As_2$ was attributed a SDW transition[4, 18].

The effect of the tin on the coupled transitions must also be considered (see Figure 1.8). The coupled transition occurs at ∼85 K for Sn flux $BaFe_2As_2$. The orthorhombic distortion transition can be clearly be seen for Sn flux $BaFe_2As_2$ (see Figure 1.2) but the presence of the SDW transition is however debatable. Sn Flux single crystals of $BaFe_2As_2$ show an 85 K magnetic transition when two Curie-Weiss curves are fitted to the magnetic susceptibility curve at high and low temperature[5]. Below the magnetic transition, the temperature parameter in the Curie-Weiss fit was approximately -5 K indicating the presence of antiferromagnetism while the temperature parameter was found to be 20 K above the transition indicating the paramagnetic behavior[5]. Sun *et al.*[22] suggested that the addition of Sn modifies the SDW transition from first-order in self flux/polycrystalline samples to second-order in Sn flux samples[22]. Wilson *et al.*[27] proposed that the Sn impurities may be masking the underlying SDW and it's magnetic ordering[27]. Thus the the exact nature of the magnetic transition at 85 K remains unclear.

1.2.3 Anisotropic Magnetization

Anisotropic magnetic susceptibility was first observed by Wang *et al.*[4] and Ni *et al.*[5] while studying single crystals of $(Ba_{1-x}K_x)Fe_2As_2$. Both groups discovered that in-plane ($H \perp c$) susceptibility was higher than out of plane ($H \| c$) susceptibility[4]. Even when the demagnetization factor was considered, the magnetic anisotropy between the in-plane and out of plane measurements was still observed[4]. Ni *et al.*[5] observed that the anisotropic susceptibility occurred below 100 K with the high temperature portion of the curves agreeing, see Figure 1.10[5]. Wang *et al.*[4] observed completely anisotropic curves for the in-plane susceptibility and out of plane susceptibility, see Figure 1.11. When comparing Figure 1.10 and 1.11, the most striking difference occurs at low temperature where the possible effect of Sn inclusion is the most significant, i.e. the Curie-Weiss paramagnetic behavior. The only similarity between the two figures was the larger magnetization observed in the in-plane measurements below the magnetic transition. But the anisotropic properties of $BaFe_2As_2$ and the differences in the magnetic susceptibility curves have yet to be studied in detail and thus the exact nature of these effects are not completely understood.

[4]In-plane susceptibility is measured when the single crystal's ab plane is parallel to the applied magnetic field **H**. Out of plane susceptibility is measured when the single crystal's ab plane is normal to the applied magnetic field **H**.

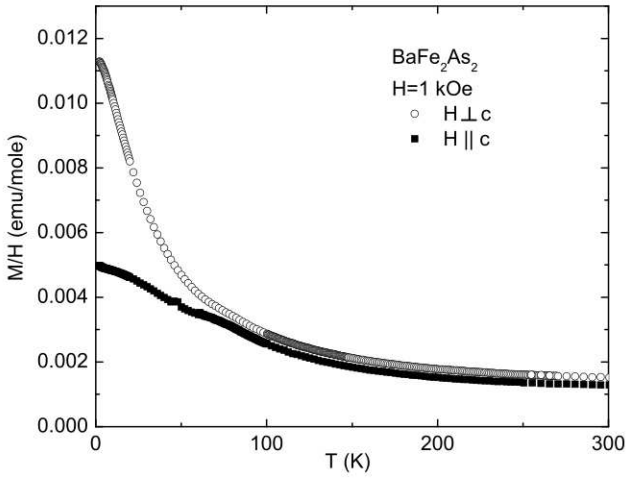

Figure 1.10: The in-plane ($H \perp c$) and out of plane ($H \| c$) magnetic susceptibilities for Sn flux single crystals of $BaFe_2As_2$ where $H = 1000$ G. Reprinted from [5].

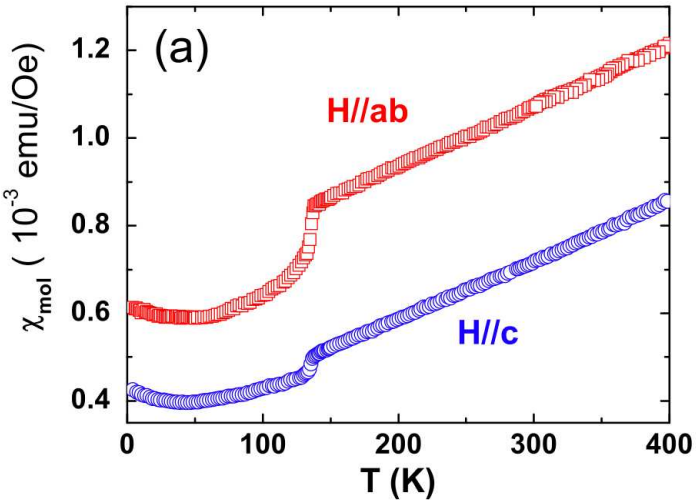

Figure 1.11: The in-plane ($H \| ab$) and out of plane ($H \| c$) magnetic susceptibilities for self flux single crystals of $BaFe_2As_2$ where $H = 65000$ G. Reprinted from [4].

1.3 Superconductivity in $(Ba_{1-x}K_x)Fe_2As_2$

Superconductivity in $BaFe_2As_2$ compound can be induced by two methods: chemical doping [21, 28] and/or the application of pressure[29]. The highest T_c superconductors containing barium, iron and arsenic can be seen in Table 1.2. The addition of a chemical dopant and/or the application of pressure on $BaFe_2As_2$ results in the suppression of the SDW and hence the reduction of magnetic order[21, 30]. Superconductivity is observed when the magnetic order is sufficiently weak thus superconductivity and weak magnetic order can still coexist[21, 29, 30]. The exact mechanism for the emergence of superconductivity is however still unknown.

1.3.1 Chemical Doping

Chemical doping in $BaFe_2As_2$ can be achieved by doping the barium, iron or arsenic sites in the crystal structure[21, 28, 31]. The crystal structure of all of the compounds in Table 1.2 is tetragonal I4/mmm but the effect of doping on the lattice parameters **a** and **c** changes depending on the sites that are replaced through doping. When the FeAs layer is doped by Ni, Co, or P, the **a** and **c** lattice parameters are both observed to decrease[28] as the dopant concentration increases. When potassium is used to dope the barium sites, the **a** lattice parameter is observed to decrease while the **c** lattice parameter increases as the potassium concentration increases, see Figure 1.4[21]. However, the changes in the lattice parameters of $(Ba_{1-x}K_x)Fe_2As_2$ are quite small since the unit cell volume does not change[5]. Instead, the As-Fe-As bond angle ε and the length of the Fe-Fe bonds are significantly changed (Figure 1.4). The bond angle ε and bond length change due to the loss of the electrons causing the Fermi surface to be less occupied[17].

[5] $BaFe_2As_2$ has a unit cell volume of 203.86 Å^3 while KFe_2As_2 has a unit cell volume of 203.49 Å^3.

Table 1.2: The highest T_c's of superconductors containing the fundamental elements of barium, iron and arsenic belonging to the AFe_2As_2 compounds. The crystal structure of all compounds is tetragonal I4/mmm.

Compound	Condition for Superconductivity	Reference
$BaFe_2As_2$	Pressure – 40 kbar with a $T_c \approx 29$ K	Alireza *et al.*[29]
$(Ba_{1-x}K_x)Fe_2As_2$	Hole-doped with a $T_c \approx 38$ K for $x \approx 0.4$	Rotter *et al.*[21]
$Ba(Fe_{1-x}Co_x)_2As_2$	Electron-doped with a $T_c \approx 23$ K for $x \approx 0.074$	Tanatar *et al.*[32]
$BaFe_{2-x}Ni_xAs_2$	Electron-doped with a $T_c \approx 21$ K for $x \approx 0.10$	Li *et al.*[31]
$BaFe_{2-x}Ru_xAs_2$	Isovalent doping with a $T_c \approx 21$ K for $x \approx 0.75$	Paulraj *et al.*[33]
$BaFe_2(As_{1-x}P_x)_2$	Isovalent doping with a $T_c \approx 30$ K for $x \approx 0.35$	Jiang *et al.*[28]
$Ba(Fe_{1-x}Rh_x)_2As_2$	Isovalent doping with a $T_c \approx 23$ K for $x \approx 0.057$	Ni *et al.*[34]
$Ba(Fe_{1-x}Pd_x)_2As_2$	Hole-doped with a $T_c \approx 17$ K for $x \approx 0.043$	Tanatar *et al.*[34]

The most critical factor for the observation of superconductivity in $BaFe_2As_2$ is the suppression of the SDW and its resulting magnetic order. When $BaFe_2As_2$ is doped by nickel, cobalt, potassium or phosphorous, the temperature of the SDW transition is observed to decrease and the SDW eventually disappears completely as the amount of dopant is increased. Johrendt *et al.*[17] observed the total suppression of the SDW in $(Ba_{1-x}K_x)Fe_2As_2$ using ^{57}Fe Mössbauer spectroscopy[6] (see Figure 1.12)[7].

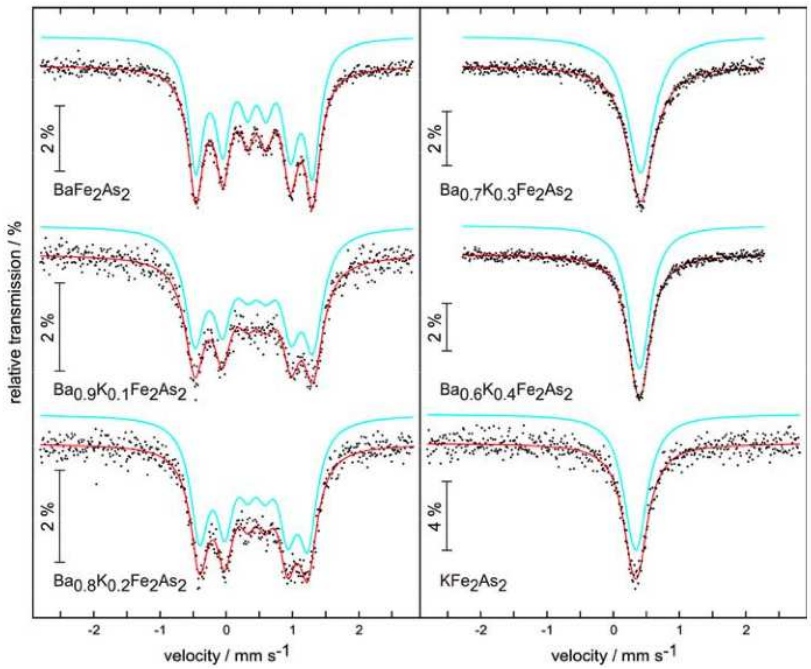

Figure 1.12: ^{57}Fe Mössbauer spectroscopy at 4.2 K for $(Ba_{1-x}K_x)Fe_2As_2$ with the empirical data and theoretical fit. Reprinted from [17].

[6]Fe Mössbauer spectroscopy uses a γ-ray source and the doppler effect to vary the incident energy on the sample. The incident γ-ray photons interacts with the spin of the electrons of the Fe atoms producing an recoil free emission of a γ-ray photons The transmitted number of γ-ray photons for each energy are measured by a detector[35]. For a more detailed explanation of Mössbauer spectroscopy, see the references in Appendix A.

[7]In Figure 1.12, the SDW is observed indirectly through it's resulting antiferromagnetic order.

The total suppression of the SDW can be observed in Figure 1.12 due to the lack of the quadrupole splitting[8]. For $x \geq 0.3$, the SDW transition disappears (i.e. no quadrupole splitting is observed). For $x < 0.3$, the superconductivity can coexist with the SDW, see the phase diagram (Figure 1.5 on p. 7). In the phase diagram, it can also be seen that the coupled transition occurs for $x < 0.3$ and furthermore the superconductivity is observed for $x = 0.1$ and 0.2 albeit the T_c's are low (i.e. 3 K for $x = 0.1$ and 25 K for $x = 0.2$)[21].

The effect of Sn on the superconductivity observed in $(Ba_{1-x}K_x)Fe_2As_2$ is another important factor due to its effect on the the coupled transition. The magnetic susceptibilities of polycrystalline and a Sn flux single crystal of $(Ba_{1-x}K_x)Fe_2As_2$ are seen in Figures 1.13 and 1.14, respectively. In Figure 1.13, the superconducting transition for polycrystalline $(Ba_{0.60}K_{0.40})Fe_2As_2$ was observed to be sharp with a T_c of 38 K. In Figure 1.14, the superconducting transition of Sn flux $(Ba_{0.55}K_{0.45})Fe_2As_2$ is observed to be broad with a lower transition temperature ($\sim$ 28 K). The lower transition temperature Sn flux $(Ba_{0.55}K_{0.45})Fe_2As_2$ was mostly caused by the loss of potassium during the single crystal growth. Even though the superconducting transition temperature for Sn flux $(Ba_{0.55}K_{0.45})Fe_2As_2$ is lower and the width of the transition is larger, it was concluded that Sn does not affect the superconductivity significantly (i.e stabilized superconductivity is still observed)[5].

[8]Quadrupole splitting (QS) is observed when the number of electrons in the d_{z^2} and $d_{x^2y^2}$ or d_{xy} and (d_{xz}, d_{yz}) orbitals are imbalanced[36]. In other words, QS is observed if the charge density around the Mössbauer nucleus is asymmetric. For Fe Mössbauer spectroscopy, the QS is enhanced due to the magnetic splitting of the energy level as a result of antiferromagnetic ordering[37]. The absence of QS implies that the antiferromagnetism is no longer present and thus the SDW is suppressed.

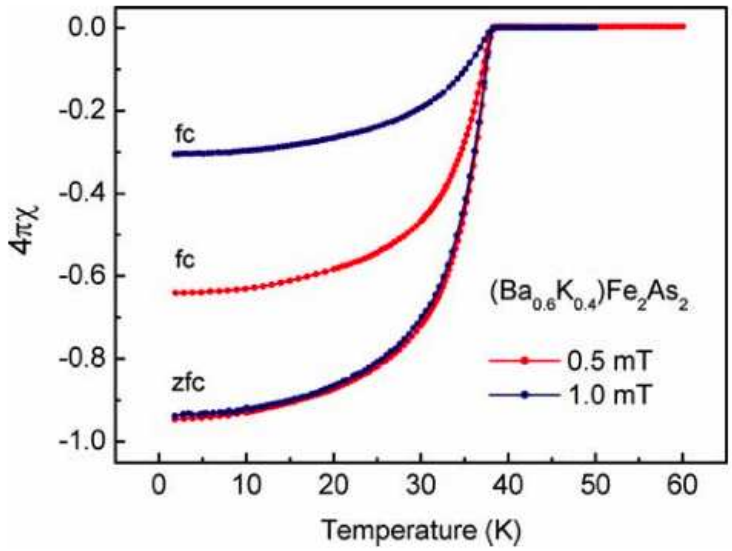

Figure 1.13: The zero field cool (zfc) and field cool (fc) magnetic susceptibilities of polycrystalline $(Ba_{0.60}K_{0.40})Fe_2As_2$. Reprinted from [17].

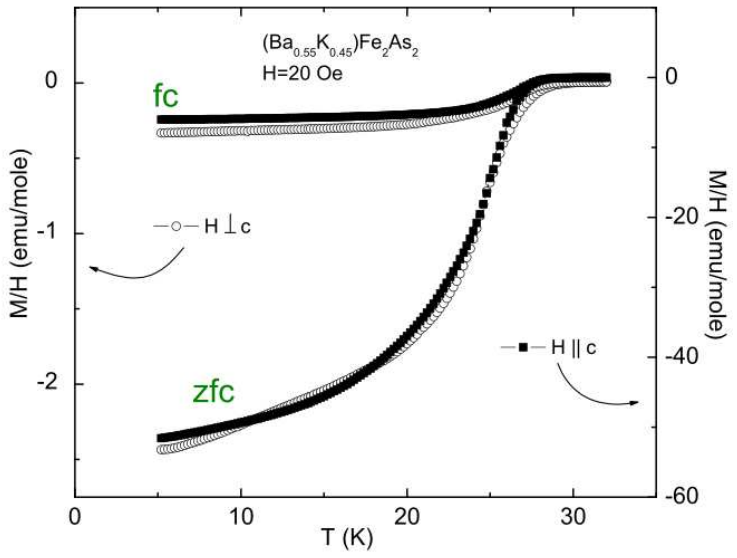

Figure 1.14: The zero field cool (zfc) and field cool (fc) magnetic susceptibilities of a Sn flux single crystal of $(Ba_{0.55}K_{0.45})Fe_2As_2$ showing the out of plane and in-plane measurements. Reprinted from [5].

1.3.2 Application of Pressure

The possibility of enhancing the superconductivity in Iron Arsenic compounds by pressure was first realized by Takahashi *et al.*[2] while studying La(O/F)FeAs. At ambient pressure, La(O/F)FeAs has a T_c of 26 K and under applied pressure the T_c increases to 46 K at $\sim$ 4 GPa or 40 kbar[2]. In the non-doped[9] AFe_2As_2 compounds, superconductivity under applied pressure (see Figure 1.16) is observed for $CaFe_2As_2$ ($T_c \approx$ 12 K at 0.2 GPa)[38], $EuFe_2As_2$ ($T_c \approx$ 29.5 K at 2 GPa)[39], $BaFe_2As_2$ ($T_c \approx$ 29 K at 4 GPa) and $SrFe_2As_2$ ($T_c \approx$ 27 K at 3 GPa)[29]. The application of pressure on doped superconducting AFe_2As_2 compounds can either decrease or increase the maximum T_c depending on the amount of dopant present, see Figure 1.17. In other words, if the doped superconducting AFe_2As_2 compound has the optimal (i.e. the highest possible T_c) or under doped then the application of pressure will increase the T_c. But if the compound is overdoped, the T_c will decrease with pressure[38, 40–42].

The most important property when considering the superconductivity under pressure observed in $BaFe_2As_2$ and similar compounds is the suppression of the SDW transition with applied pressure. Torikachvili *et al.*[40] proposed that the complete suppression of the SDW transition should occur around 80 kbar or 8 GPa based on extrapolation of their data[40]. Fukazawa *et al.*[30] measured the evolution of T_c and T_{SDW} for $BaFe_2As_2$ using resistivity measurements to find the transition temperatures, see Figure 1.15. In Figure 1.15, the SDW transition temperature reaches a minimum of $\sim$ 70 K at 9.0 GPa while the maximum T_c of 30 K occurs at $\sim$ 4 Gpa with coexistence of the SDW. Furthermore, it was observed that the complete suppression of the SDW occurs around 9 to 13 GPa yielding a superconducting T_c between 15 K and 20 K[30]. Alireza *et al.*[29] measured the T_c as a function of temperature using

[9] These compounds are non-superconductors at ambient pressure.

magnetic susceptibility up to 6 GPa or 60 kbar and constructed a T-P phase diagram for $BaFe_2As_2$ and other AFe_2As_2 compounds, see Figure 1.16. In Figure 1.16, it can clearly be seen that the maximum T_c is be observed to 30 K at $\sim$ 4 GPa or 40 kbar for $BaFe_2As_2$[29].

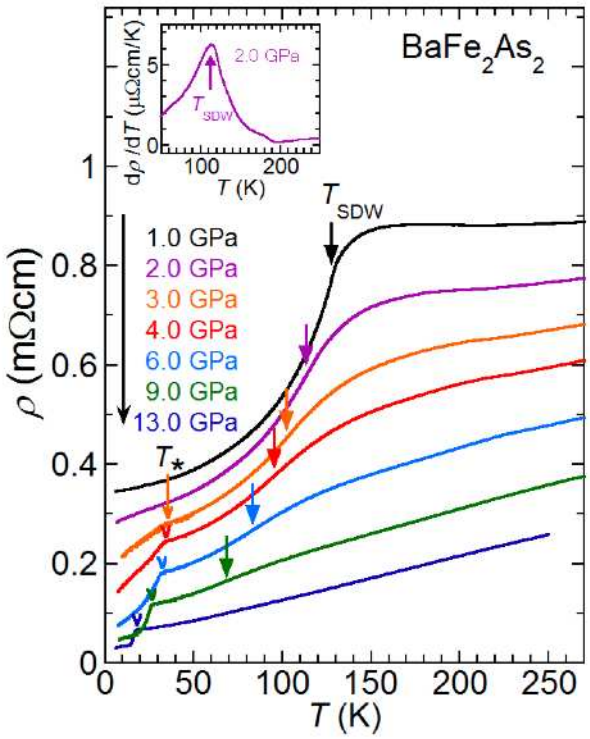

Figure 1.15: The temperature dependence of the resistivity for $BaFe_2As_2$ under an applied pressure from 1.0 GPa to 13 GPa. The SDW transition temperature is denoted by T_{SDW} while the superconducting transition temperature is denoted by T_*. Reprinted from [30].

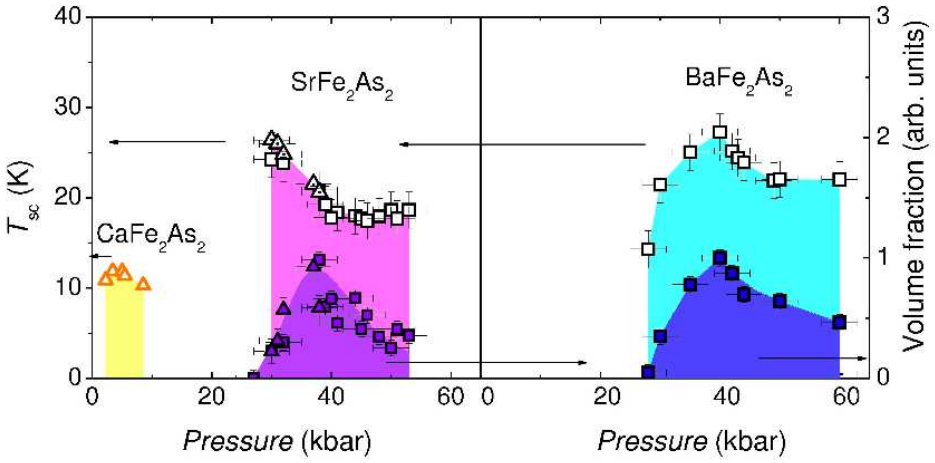

Figure 1.16: The pressure dependence of the T_c and volume fraction for AFe_2As_2 compounds which are superconducting under pressure. Reprinted from [29].

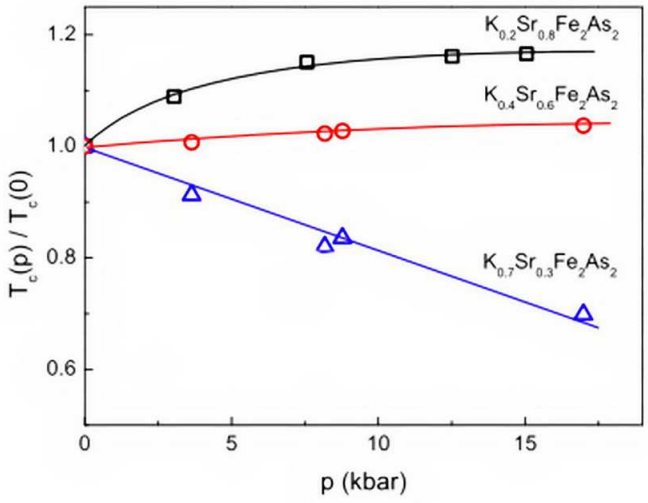

Figure 1.17: The effect of pressure on the T_c of underdoped (Black or open squares), nearly optimal doped (Red or open circles) and overdoped (Blue or open triangles) samples of $K_{1-x}Sr_xFe_2As_2$, where $T_c(p)$ represents the T_c under pressure and $T_c(0)$ represents the T_c at ambient pressure. Reprinted from [42].

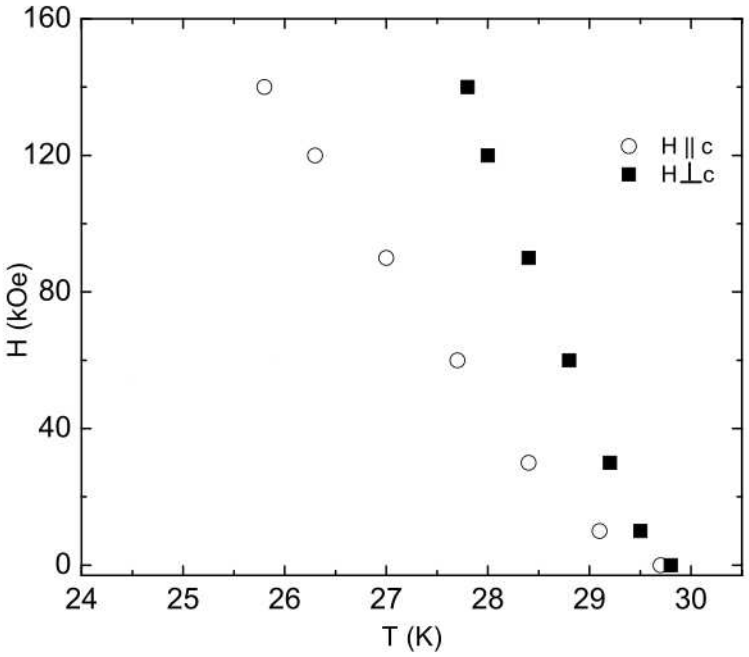

Figure 1.18: The high critical field, $H_{c_2}(T)$, curves for the in-plane (H⊥c) and out of plane (H∥c) orientations using up to 140 kG or 14 T for a Sn flux single crystal of $(Ba_{0.55}K_{0.45})Fe_2As_2$. Reprinted from [5].

1.3.3 Anisotropic Critical Fields

After growing the first single crystals of $(Ba_{1-x}K_x)Fe_2As_2$, Ni *et al.*[5] observed highly anisotropic behavior in the high critical field limit H_{c_2}(T) when measuring the resistivity of single crystals with a magnetic field up to 14 T. The anisotropic high critical field plot can be seen in Figure 1.18. In Figure 1.18, it can clearly be seen that in-plane curve increases at a faster rate than out of plane and hence when the data was extrapolated the anisotropy became quite significant (i.e. $\gamma = \frac{H_{c_2}^{\perp c}}{H_{c_2}^{\parallel c}} \sim 3.5$). Furthermore from an extrapolation of the data in Figure 1.18, it was found that the out of plane high critical field could be between 75 and 140 Telsa[5]. Yuan[43] performed a similar experiment with magnetic fields up to 60 Telsa, see Figure 1.19.

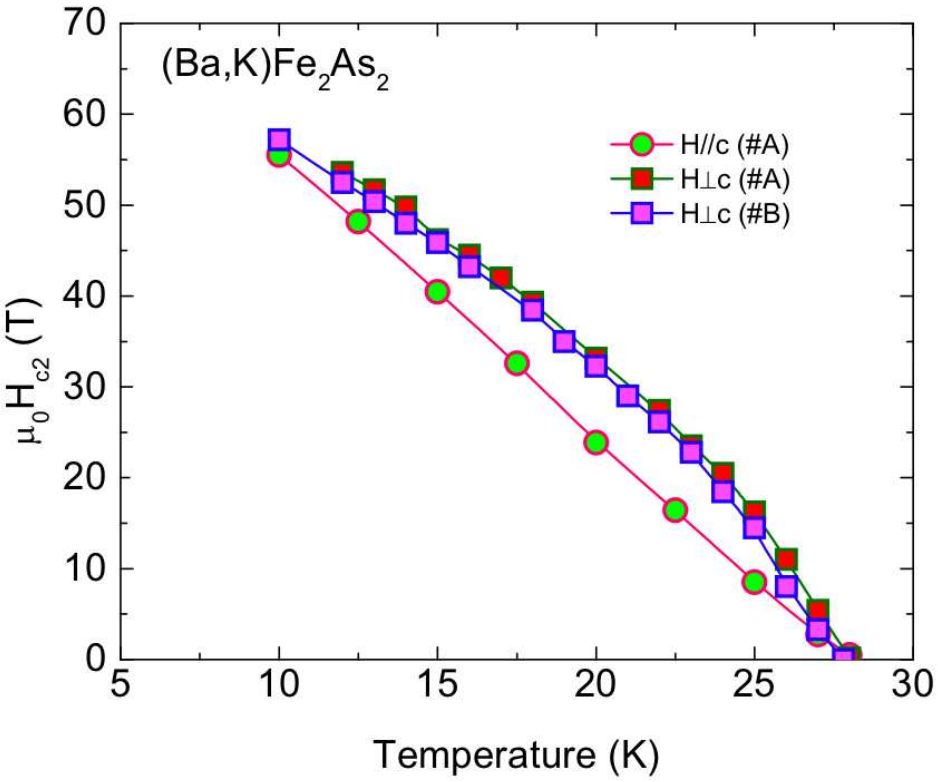

Figure 1.19: The high critical field, $H_{c_2}(T)$, curves for the in-plane (H⊥c) and out of plane (H‖c) orientations using up to 60 T for a self flux single crystal of $(Ba_{0.60}K_{0.40})Fe_2As_2$. Reprinted from [43].

In Figure 1.19, it was found that the anisotropy was significantly less than proposed by Ni *et al.*[5]. It can clearly be seen that the initial curvature in the in-plane curve observed in Figure 1.18 levels off and increases monotonically in an almost linear behavior. Furthermore, the extrapolated upper critical field H_{c_2}(T) with out of plane from Figure 1.19 is estimated to be larger than 100 T which is within the range proposed by Ni *et al.*[5].

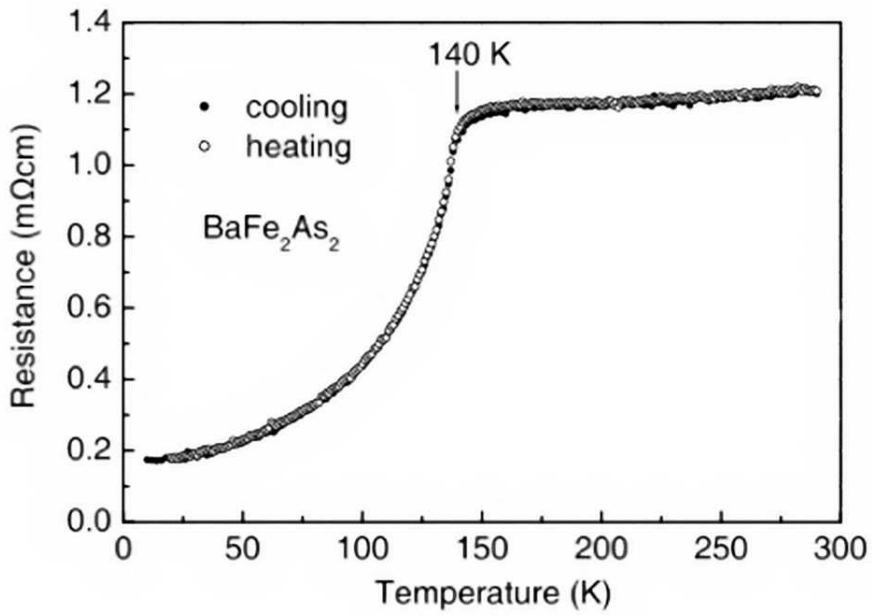

Figure 1.20: The temperature dependence of the resistivity for polycrystalline $BaFe_2As_2$ with the heating and cooling curves. Reprinted from [18].

1.4 Resistivity of $(Ba_{1-x}K_x)Fe_2As_2$

The resistivity of $BaFe_2As_2$ is strongly characterized by the the SDW transition and anisotropic properties. The resistivity of polycrystalline $BaFe_2As_2$ can be seen in Figure 1.20. In Figure 1.20, the SDW transition can clearly be seen at 140 K and furthermore $BaFe_2As_2$ can be characterized as a poor-metal due to the higher resistivity (1 $m\Omega \cdot cm$ at 300 K)[18]. The resistivity of $BaFe_2As_2$ single crystals grown using self flux and Sn flux method can be seen in Figure 1.21. In Figure 1.21, a transition is observed for Sn flux single crystals around 85 K but it is unclear if this transition can be attributed to the SDW. The self flux single crystals of $BaFe_2As_2$ and polycrystalline $BaFe_2As_2$ have similar resistivity curves with the SDW transition at $\sim$140 K[18, 22]. Furthermore, anisotropic resistivity can also be observed in single crystals of $BaFe_2As_2$. Wang *et al.*[4] measured the in-plane and out of plane resistiv-

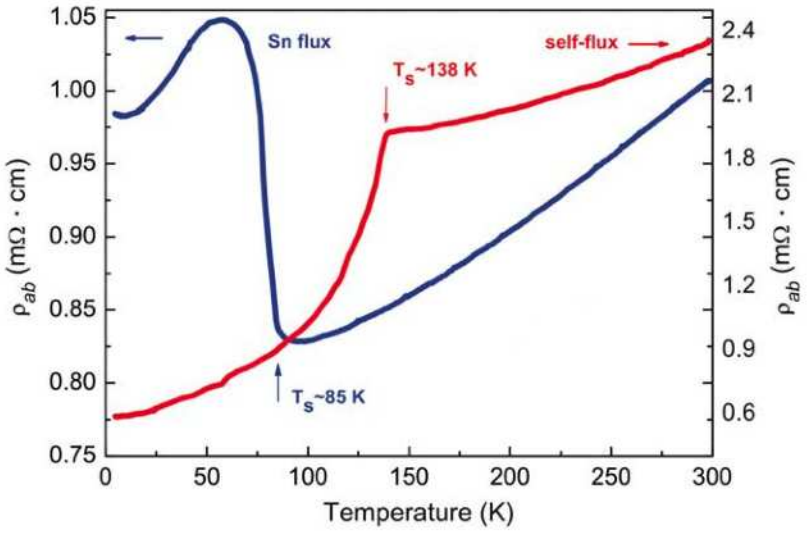

Figure 1.21: The temperature dependence of the in-plane resistivity for Sn flux and self flux single crystals of $BaFe_2As_2$. Reprinted from [22].

ity of self flux $BaFe_2As_2$ single crystals (see Figure 1.22). They found that the ratio of the out of plane to in-plane resistivity, $\frac{\rho_c}{\rho_{ab}}$, was approximately 150 for the whole temperature range.

When superconductivity is induced in $BaFe_2As_2$ by chemical doping or the application of pressure, metallic behavior is observed with an abrupt drop in resistivity near the superconducting transition. At the low levels of doping the SDW transition can also be seen. The effect of doping the FeAs sheets or the barium site can be be seen in Figures 1.23 and 1.24, respectively. The SDW transition temperature is observed to decrease and eventually disappear as the amount of dopant, x, is increased[21, 28, 31, 44]. The broad humps in Figure 1.23 are due to the SDW transition[31, 44], but so far this broad transition has only been seen in single crystals.

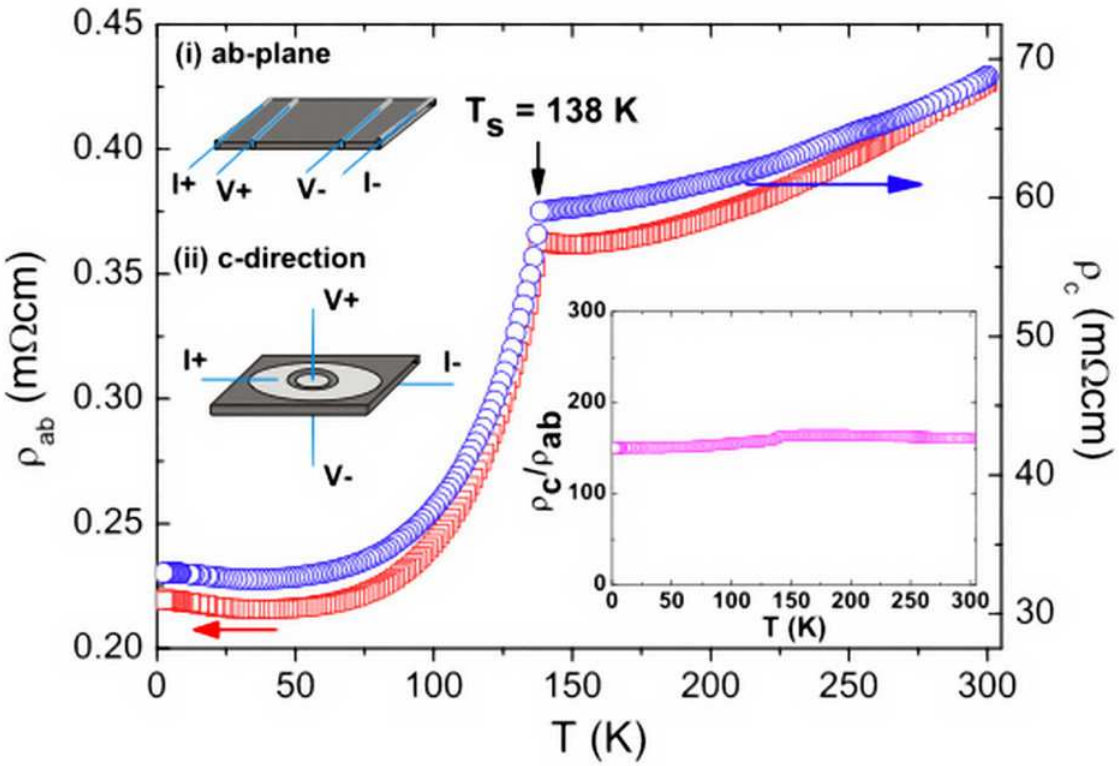

Figure 1.22: The temperature dependence of the in-plane and out of plane anisotropic resistivity for a self flux single crystal of $BaFe_2As_2$, where the inset figure represents the anisotropic ratio of the in-plane and out of plane resistivity. Reprinted from [4].

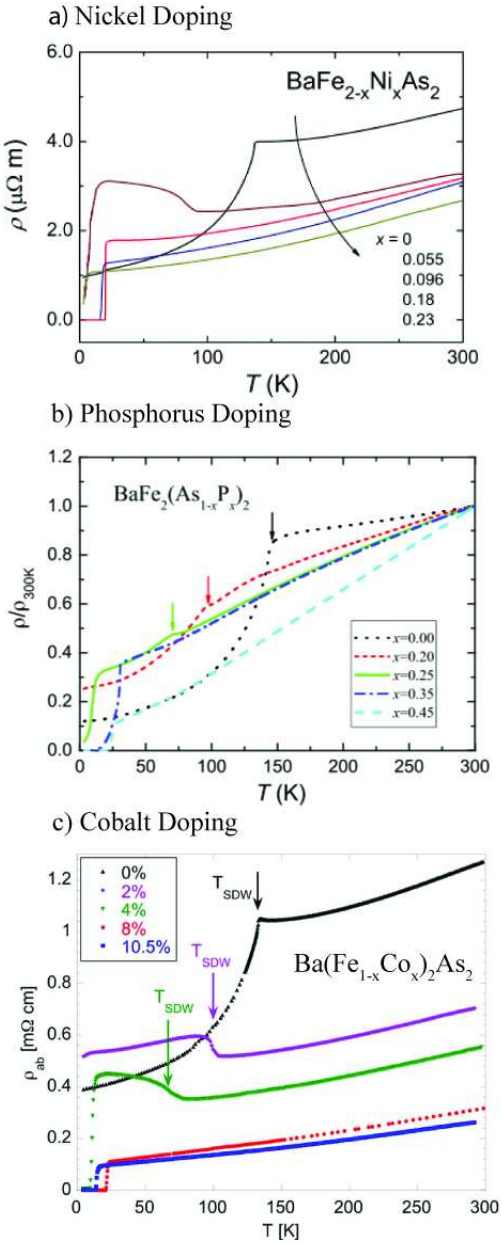

Figure 1.23: The temperature dependence of the in-plane resistivity for a single crystal self flux single crystal nickel, polycrystalline phosphorus and a self flux single crystal of cobalt doped $BaFe_2As_2$. Reprinted from [28, 31, 44].

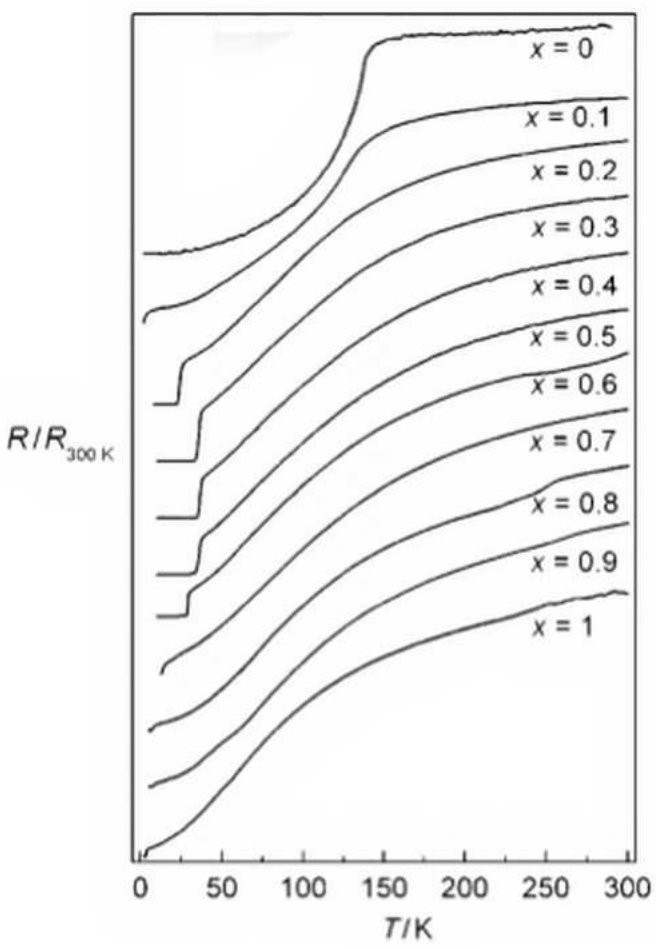

Figure 1.24: The temperature dependence of the in-plane resistivity for polycrystalline $(Ba_{1-x}K_x)Fe_2As_2$. Reprinted from [21].

1.5 General Outline of the Thesis

The main goal of this thesis was to improve the quality and superconductivity of Sn flux crystals of $(Ba_{1-x}K_x)Fe_2As_2$. The rapid heating method[45] was used to improve the superconductivity through the minimization of potassium loss. The presence of multiple phases in single crystals was observed and the effect of these phases on transport and magnetic properties were studied.

The thesis layout is as follows:

- **Chapter 2 – Sample Preparation**: The polycrystalline and the flux methods of the preparation and the effect of potassium on the chemical synthesis are discussed. The rapid heat Sn flux method used to grow the single crystals for this thesis is also discussed.

- **Chapter 3 – Results and Discussion**: Energy dispersive X-ray spectroscopy and single crystal X-ray diffraction analysis of the grown single crystals are discussed. The temperature and field dependent magnetization measurements are discussed. The effect of annealing on the magnetization of the single crystals is discussed. The resistivity measurements for the single crystals are discussed.

- **Chapter 4 – Conclusion**: The summary of the results are presented.

- **Appendix A** – Additional references for SQUID Magnetometry, Spin Density Waves and Mössbauer Spectroscopy are presented.

Chapter 2

Sample Preparation

The primary methods used to synthesize $BaFe_2As_2$ or $(Ba_{1-x}K_x)Fe_2As_2$ are the solid state and the flux methods. The solid state method produces polycrystalline samples while the flux methods produce single crystals. $(Ba_{1-x}K_x)Fe_2As_2$ is produced when potassium is substituted for barium in the chemical synthesis. When potassium is used, it is important to consider the vaporization and reactivity of the alkaline metal. The sample preparation methods must be modified to control the amount of potassium lost due to vaporization and reactions with quartz and aluminium oxide.[1]

2.1 Synthesis of $(Ba_{1-x}K_x)Fe_2As_2$ Compounds

2.1.1 The Polycrystalline Method

Polycrystalline $BaFe_2As_2$ and $(Ba_{1-x}K_x)Fe_2As_2$ can be prepared by using the solid state reaction method. Barium, iron and arsenic are mixed according to molar ratios and placed in an aluminum oxide crucible. The crucible is then placed in a quartz tube and evacuated. The quartz tube is filled with argon gas and sealed to produce a quartz ampoule. The sample is heated, annealed and sintered at 850 ^{o}C, 900^{o}C and 700 ^{o}C, respectively. In the annealing and sintering step, the ampoule must be shattered and the sample must be removed from the crucible. The sample is then rehomogenized using a mortar and pestle. The homogenized sample is then

[1]Quartz and aluminium oxide are used in the sample preparations method as sample containers.

placed in the same crucible but sealed in a new argon filled quartz ampoule[18]. When doping with potassium, the heating, annealing and sintering temperatures change to 600 ^{o}C, 652^{o}C and 750 ^{o}C, respectively. The partial control of potassium losses can be achieved by the reducing the synthesis temperatures and filling the ampoule with 1/3 atm. of argon gas[3].

2.1.2 The Flux Methods

The flux methods were discovered by H. Moissan in 1904. H. Moissan *et al.*[46] produced single crystals of 'Diamonds'[2] using a liquid iron flux and other metallic fluxes[46]. The use of the Sn flux method dates back to 1910, when P. Jolibois and C. R. Hebd[47] grew single crystals of nickel phosphides in a Sn flux. When growing compounds with any flux method, it is important that no stable compounds can be formed between the flux and the materials involved in the crystal growth. This method allows the crystal growth to occur at lower temperatures and the elements or compounds do not have to dissolve fully in the flux. The flux acts as a transport medium which allows the various elements or compounds to flow together and form the desired single crystals[46]. To protect the flux and other components during the crystal growth, the materials are placed in an aluminum oxide crucible which is then sealed in a quartz ampoule. A quartz ampoule can be used when the temperatures do not exceed 1200 ^{o}C and less than 5 ml of material is used. The quartz ampoule is used to contain any reactive elements/compounds(i.e. potassium). The molten flux can be separated from the single crystals by tilting and decanting the quartz ampoule. The quartz ampoule provides an enclosed vessel to easily separate the flux from the single crystals[48].

[2]H. Moissan actually grew small crystals of SiC or Moissanite.

Two fluxes can be used to grow single crystals of $BaFe_2As_2$ and $(Ba_{1-x}K_x)Fe_2As_2$: FeAs or Sn. Both pre-reacted and elemental mixtures can be used with the flux methods. Both flux methods produce single crystals but the Sn flux produces larger single crystals with the additional caveat of Sn incorporation in the single crystals. Similar potassium controls can be used as discussed for the polycrystalline method[4, 5, 17].

2.2 Sn Flux Method

In the Sn flux method, the mixture of barium, arsenic, iron and potassium or the equivalent pre-reaction products can be used[17]. This method is particularly useful due to the ability to grow single crystals quickly without the use of specific furnaces and tools[48]. Furthermore, Sn was chosen as the flux since no stable binary compounds can be formed with the elements in $(Ba_{1-x}K_x)Fe_2As_2$.

The caveats of using the Sn flux method are the macroscopic inclusion of Sn(less than 1% typically) in the single crystals and the separation of the Sn from the grown single crystals. The inclusion of Sn in the single crystals is known for other $ThCr_2Si_2$ compounds such as AFe_2P_2, ACo_2P_2, and ANi_2P_2 where A are lanthanides. Furthermore, the inclusion of Sn is particularly seen when high reaction temperatures are used[48]. Traditionally, the inclusion of Sn in the single crystals was found using calorimetry measurements near the melting point of tin[46]. For $(Ba_{1-x}K_x)Fe_2As_2$, the inclusion of Sn in the single crystals has been observed using Energy Dispersive X-ray Spectroscopy[5], differential temperature analysis, and photoelectron spectroscopy [22]. The inclusion of Sn most likely results in the replacement of Fe or As in the iron arsenic planes with Sn[22]. To separate the flux from the single crystals, one of the following methods can be used: high temperature centrifuge separation, an

acidic solution or mechanical separation. The high temperature centrifuge method is used to spin off the Sn flux while the Sn is still molten (i.e. above the melting point of Sn (232 ^{o}C)). The acidic solution method dissolves the remaining Sn in dilute hydrochloric acid to produce SnCl(aq) and H_2(g). However the acidic solution can quickly damage single crystals[48] and hence this method should only be used as a last resort. The mechanical method can be used to selectively remove single crystals by force or by heating the remaining Sn flux above 232 ^{o}C, and then slowly removing the single crystals. Alternatively, a piece of double sided tape can be used to remove Sn from the top and bottom of a thick single crystal producing a clean Sn free surface.

The Sn flux method used for this thesis is a modified version of the Ni *et al.*[5] method. In the original method from Ni *et al.*[5], it was found that the amount of potassium required for doping must be doubled in order to offset the potassium lost to vaporization and undesired reactions. For the work in this thesis, the additional control of potassium loss was obtained using a rapid heating technique[45]. With the Rapid Heating technique[45] and the doubling potassium concentration, it was observed that the desired amount of potassium was present in the grown single crystals. The exact method used to grow the single crystals is as follows:

- **Step One**: When growing $(Ba_{1-x}K_x)Fe_2As_2$ single crystals, a high temperature vacuum drying system and an argon filled glovebox were used to prevent contamination. Before drying, the quartz tubes and/or the aluminium oxide crucibles were cleaned in Aqua regia(3-part hydrochloric acid, 1-part nitric acid) and subsequently washed with distilled water. Both the quartz tubes[3] and/or

[3]The quartz tubes had an inner diameter of 19 mm and a outer diameter of 23 mm with a wall thickness of 2 mm. A 19/22 outer ground standard taper quartz joint was used to connect the quartz tube to the glass closure valve.

the aluminium crucibles[4] were placed in a large quartz vacuum tube and heated to 900^{o}C under vacuum. The large quartz vacuum tube was then slowly cooled down to room temperature over five hours. The valve on the quartz vacuum tube was then closed and the cleaned tubes/crucibles were transferred to the drybox. Chemical synthesis method 2.1 or 2.2 can be used to prepare the mixture required to grow the single crystals. The mixture of the elements and/or compounds were measured in an argon filled environment (an argon filled drybox). Half of the Sn was placed at the bottom of an aluminium oxide crucible and the remaining components of the mixture was placed on top of this layer followed by the placement of the remaining Sn inside the crucible.

$$(1-x)Ba + 2xK + 2Fe + 2As + 48Sn \overset{Sn\ Flux}{\longrightarrow} (Ba_{1-x}K_x)Fe_2As_2$$

Chemical Synthesis 2.1: This chemical equation shows the Sn flux reaction when only the pure elements are used.

$$(1-x)Ba + 2xK + 2FeAs + 48Sn \overset{Sn\ Flux}{\longrightarrow} (Ba_{1-x}K_x)Fe_2As_2$$

Chemical Synthesis 2.2: This chemical equation shows the Sn flux reaction when pure elements and ferric arsenide are used, instead of Fe and As separately.

- **Step Two**: A piece of quartz wool was pushed down a preheated/dryed quartz tube and the crucible prepared in step one was then placed in the quartz tube with a piece of quartz wool on top of the crucible. A glass closure valve was connected on the top of the quartz tube and the quartz tube with the glass valve closed was removed from the dry box. The quartz tube and glass valve

[4]The aluminum oxide crucible had an inner diameter of 10 mm and a outer diameter of 15 mm with a wall thickness 2.5 mm. The crucibles were 40 mm long with a rounded bottom.

were connected to a vacuum line and roughed out by a rotary vacuum pump. The quartz tube was filled with argon and roughed out by the rotary vacuum pump again. After achieving sufficiently low vacuum, the quartz tube was then placed on the high vacuum line.

- **Step Three**: To create a closure in the quartz tube, the vacuum lines were disconnected from the quartz tube and subsequently filled with 1 atm of argon gas. To control the collapse of the quartz tube, the quartz tube was vented to the atmosphere using a continuous argon flow as the blowing gas to produce a closure. A hydrogen/oxygen torch was used to create a small closure in the quartz tube approximately 6 cm from the bottom, see Figure 2.1. The vent to the atmosphere was then closed. The quartz tube was roughed out and connected to the high vacuum line for a few hours after which the tube was filled with 1/3 atm of argon and sealed at the closure with a hydrogen/oxygen torch, producing a quartz ampoule.

- **Step Four**: The high temperature furnace was preheated to 700^{o}C and the quartz ampoule was placed in an aluminum oxide crucible which was then placed in the furnace. The rapid heating technique (see Section 2.3) was used to minimize the amount of potassium loss due to vaporization and undesired reactions. The quartz ampoule was heated to 850^{o}C over one hour and slowly cooled down to 500^{o}C over thirty-six hours. The Sn flux can be decanted at 500^{o}C after removing the quartz ampoule from the furnace, see Figure 2.2. The single crystals recovered from the flux after breaking the ampoule can be seen in Figure 2.3. A single crystal cleaned with hydrochloric acid can be seen in Figure 2.4.

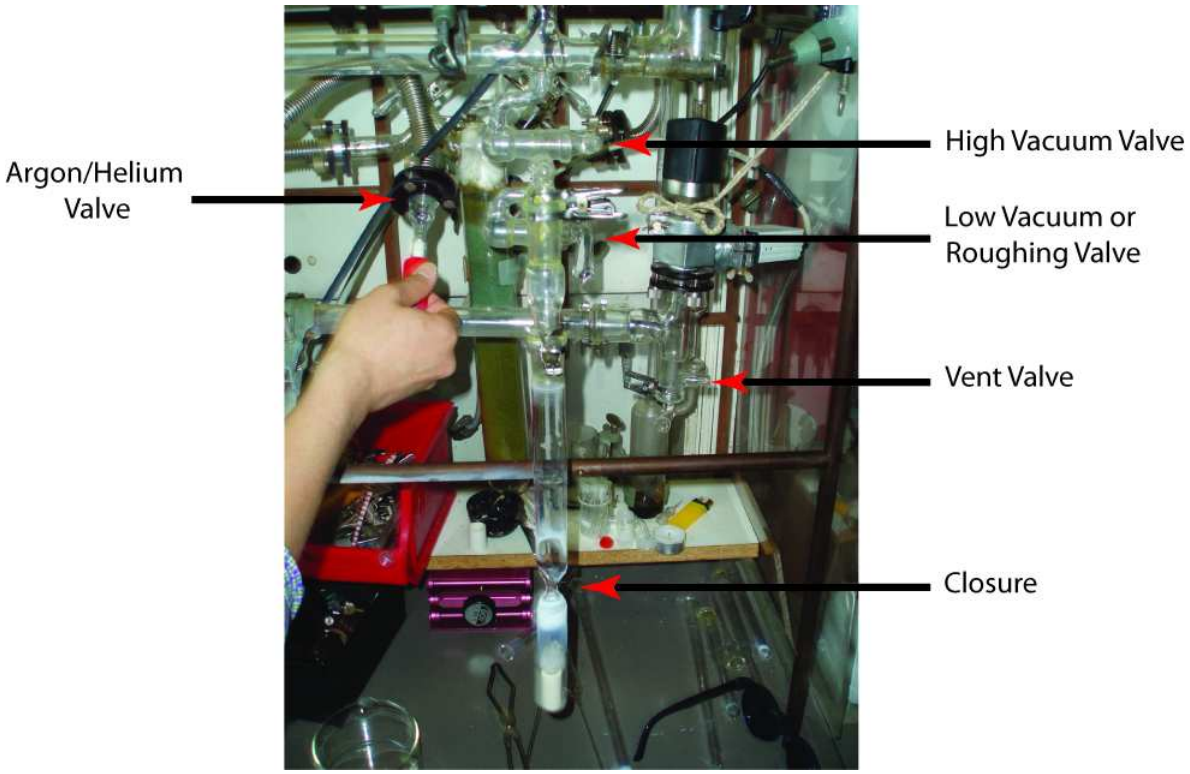

Figure 2.1: A quartz tube on the vacuum system showing the various valves and the closure on the quartz tube.

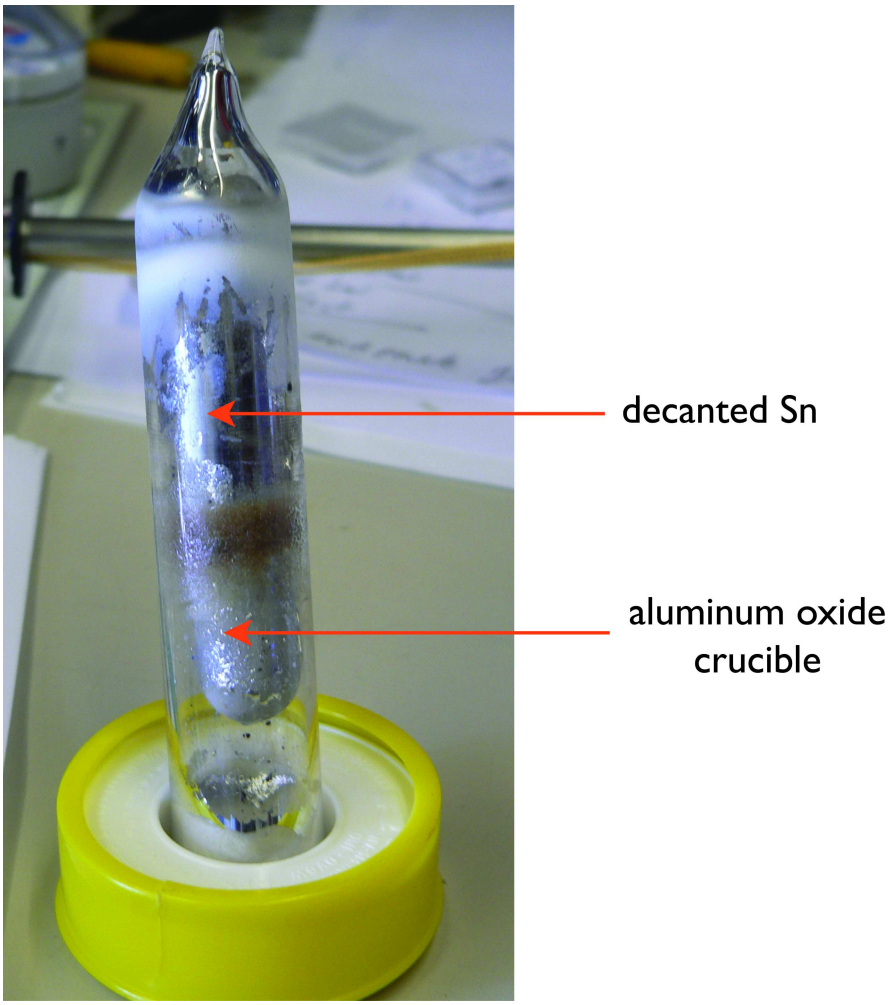

Figure 2.2: A quartz ampoule after the completion of the temperature profile seen in Figure 2.6. The Sn flux has been decanted from single crystals located in the aluminum oxide crucible.

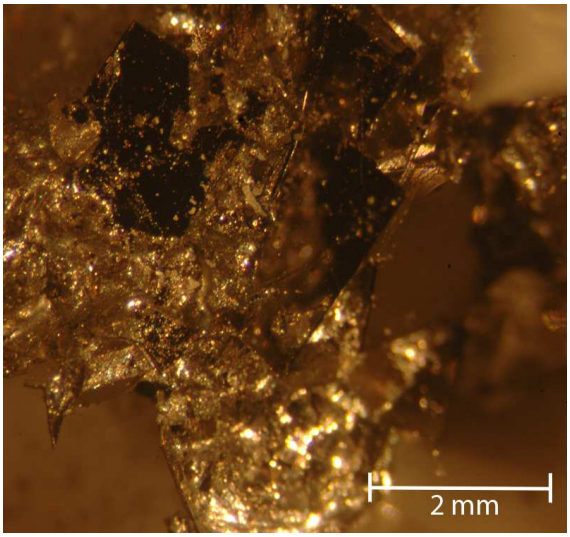

Figure 2.3: An image of single crystals from BKFA-1-NA taken using a microscope camera. The remaining Sn flux can still be seen surrounding the plate-like single crystals.

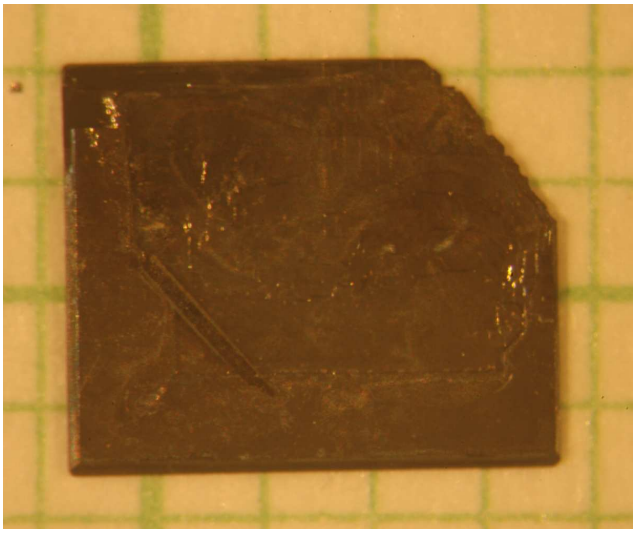

Figure 2.4: An image of a single crystal from BKFA-3-A taken using a microscope camera. The dimensions of the single crystal are approx. 3.5 mm x 5 mm x 0.26 mm.

2.3 Rapid Heating Technique and Temperature Profiles

$(Ba_{1-x}K_x)Fe_2As_2$ single crystals were grown from a Sn flux using two temperature profiles: the slow heating method (see Figure 2.5) and the rapid heating method (see Figure 2.6). The slow heating method was used to grow the first batch of single crystals (BKFA-1-NA)[5]. In the slow heating method, the ampoule was inserted at room temp and heated over five hours to 300^oC and dwelled for two hours. The ampoule was then heated from 300^oC to 850^oC for five hours and dwelled for one hour. The ampoule was then cooled down to 500^oC over thirty-six hours. Energy Dispersive X-ray Spectroscopy (EDS) was performed on single crystals from BKFA-1-NA. The EDS analysis indicated the presence of Sn, Ba, Fe and As in the single crystals. Thus it was concluded that the complete loss of potassium was due to the slow heating method and a vacuum atmosphere in the ampoule.

Due to the significant loss of potassium using the slow heating method, it was proposed that the potassium loss could be minimized if the ampoule was heated rapidly instead. Previously, the rapid heating method was used by Motohashi *et al.*[49] to control the sodium concentration in $Na_xCo_2O_4$. It was found that Na evaporates when heated slowly thus it was proposed that less sodium would be lost if $Na_xCo_2O_4$ was rapidly heated. When $Na_xCo_2O_4$ was inserted at 750^oC , it was observed that no sodium was lost due to evaporation[49]. Since potassium is also observed to evaporate and vaporize, the temperature profile was changed to minimize the amount of potassium lost due to evaporation and undesired reactions with quartz and aluminium oxide. The rapid heating method[45] was then used to the grow

[5]BKFA-1-NA was sealed under vacuum instead of 1/3 of atm argon. The target composition of BKFA-1-NA was $Ba_{0.55}K_{0.45}Fe_2As_2$.

the remaining five batches of single crystals (BKFA-2-A to BKFA-6-A). In the rapid heating method, the ampoule was inserted into the furnace at 700^{o}C and rapidly heated to 850^{o}C. Using the EDS analysis, it was observed that the desired amount of potassium was present in single crystals when the rapid heating method was used. Hence it can be concluded that the rapid heating method minimized the potassium loss during crystal growth.

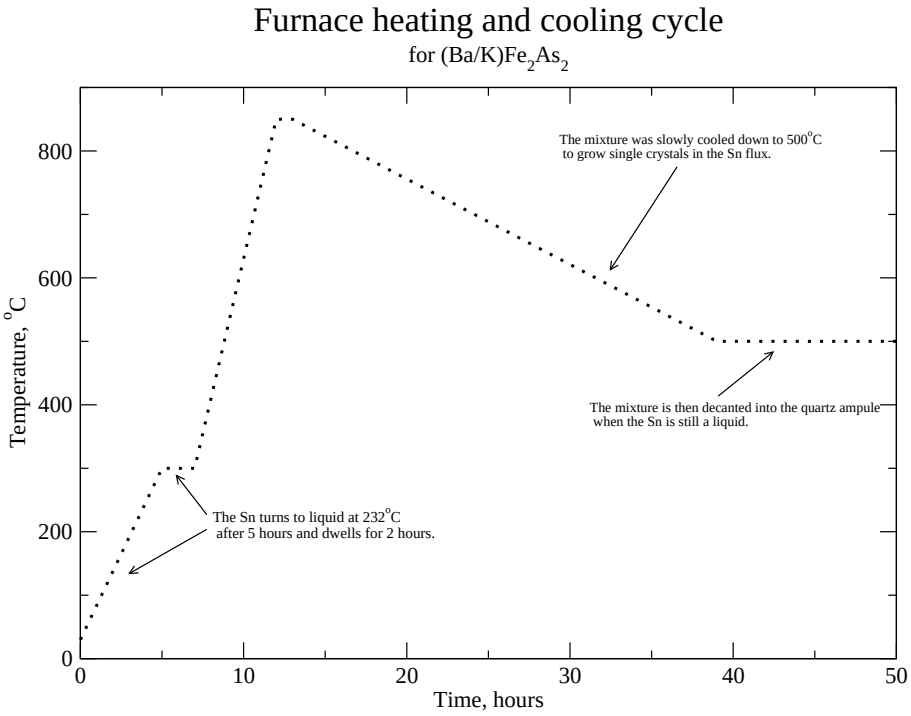

Figure 2.5: Temperature profile for the slow heating method.

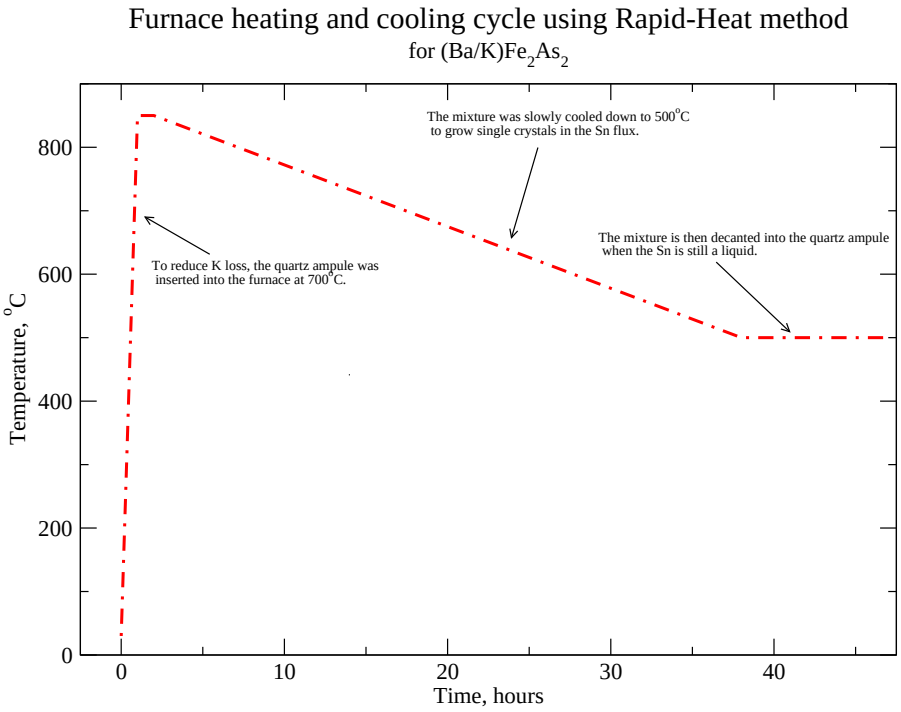

Figure 2.6: Temperature profile for the rapid heating method.

2.4 Growth Conditions for the Single Crystals

For this thesis, six single crystal batches were grown using the methods discussed in Section 2.2. The growth conditions for BKFA-1-NA to BKFA-6-A single crystals can be seen in Table 2.1. The first three single crystal batches were synthesized to determine if the ideal superconducting composition (i.e. highest possible $T_c \sim$ 38 K) could be produced using the Sn flux method. Barium and potassium atoms can occupy nine sites in total in the crystal structure. The last three single crystal batches were synthesized to determine the effect of varying the rational barium and potassium ratios on placement of barium and potassium in the crystal structure.

Table 2.1: Synthesis details for BKFA-1-NA to BKFA-6-A single crystals showing the target compound and growth conditions. The NA notation denotes that the single crystals were not grown in an argon filled ampoule while the A notations denotes that the single crystals were grown in an argon filled ampoule.

Growth	**Target Compound**	**Growth Conditions**
BKFA-1-NA	$(Ba_{0.55}K_{0.45})Fe_2As_2$	This batch was sealed under vacuum and the slow heating method was used. Chemical synthesis method 2.1 was used.
BKFA-2-A	$(Ba_{0.55}K_{0.45})Fe_2As_2$	This batch was sealed under 250 mbar of Argon and the rapid heating method was used. Chemical synthesis method 2.1 was used.
BKFA-3-A	$(Ba_{0.55}K_{0.45})Fe_2As_2$	This batch was sealed under 328 mbar of Argon and the rapid heating method was used. Chemical synthesis method 2.1 was used.
BKFA-4-A	$(Ba_{0.66}K_{0.34})Fe_2As_2$	This batch was sealed under 328 mbar of Argon and the rapid heating method was used. Chemical synthesis method 2.1 was used.
BKFA-5-A	$(Ba_{0.33}K_{0.67})Fe_2As_2$	This batch was sealed under 328 mbar of Argon and the rapid heating method was used. Chemical synthesis method 2.1 was used. Potassium loss was observed due to a malfunction of the furnace.
BKFA-6-A	$(Ba_{0.25}K_{0.75})Fe_2As_2$	This batch was sealed under 328 mbar of Argon and the rapid heating method was used. Chemical synthesis method 2.2 was used.

Chapter 3

Results and Discussion

3.1 Energy Dispersive X-ray Spectroscopy

The Energy Dispersive X-ray Spectroscopy (EDS) Analysis was performed using a scanning electron microscope with an Oxford Inca EDS microprobe analyzer[1]. EDS analysis was used as a tool to determine the composition of the grown single crystals. The homogeneity of the grown single crystals was also studied by the randomly selecting single crystals from the batches. The EDS analysis for BKFA-1-NA to BKFA-6-A can be seen in Tables 3.1 and 3.2[2]. The EDS analysis clearly shows presence of potassium in BKFA-2-A to BKFA-6-A, where the rapid heating method was used. It was observed that BKFA-2-A, BKFA-5-A and BKFA-6-A were inhomogeneous due the presence of multiple compositions in the crystal batches. No Sn was detected in BKFA-2-A to BKFA-6-A but Sn was present in BKFA-1-NA (see Figure 3.1). The presence of approximately 3% Sn in BKFA-1-A is due to the incomplete cleaning of Sn coating the surface of the single crystal.

[1] A LN_2 cooled Si(Li) detector was used in the Oxford Inca EDS microprobe analyzer. Boron was the lowest element which could be detected by Si(Li) detector.

[2] The multiple compositions for BKFA-2-A, BKFA-5-A and BKFA-6-A in Tables 3.1 and 3.2 were measured on different single crystals.

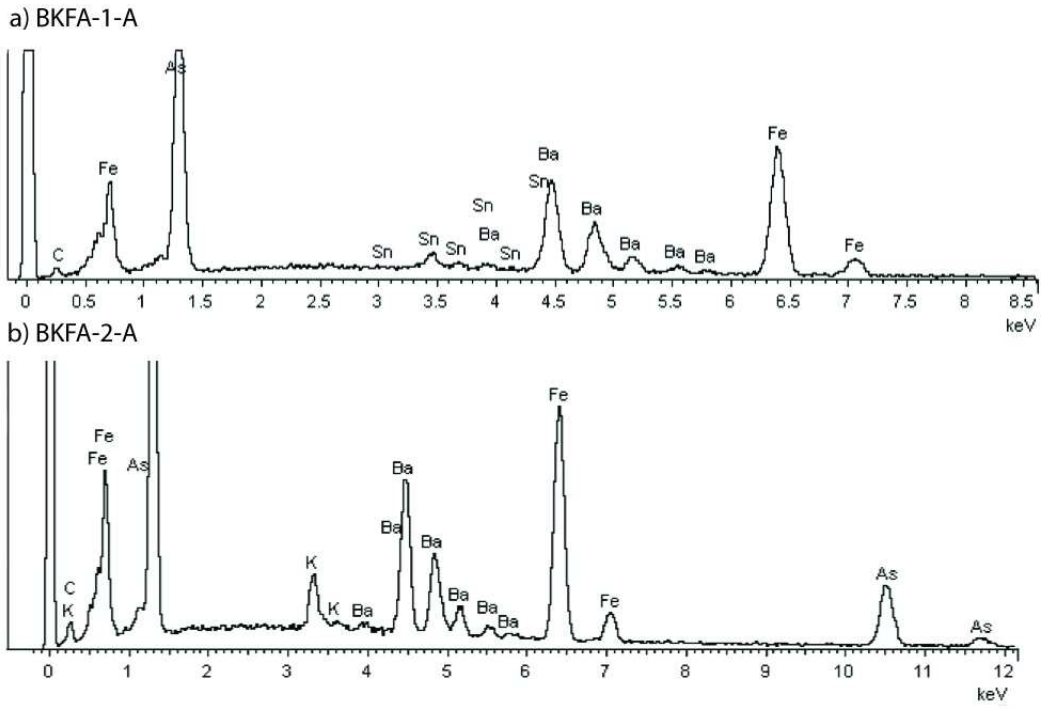

Figure 3.1: Energy Dispersive X-ray Spectroscopy spectra of BKFA-1-NA and BKFA-2-A. Both spectra have an arbitrary scale relative to the calibration standards.

Table 3.1: The EDS analysis for BKFA-1-A to BKFA-3-A and BKFA-5-A showing the atomic % of each element, the empirical chemical formula and all associated errors values. The associated errors were determined using the standard deviation from multiple EDS measurements points. The italic compositions are the dominant compositions for BKFA-2-A and BKFA-5-A.

BKFA-1-A $\sim Ba_{1.00\pm0.04}Sn_{0.037\pm0.005}Fe_{2.28\pm0.05}As_{2.13\pm0.03}$			
Ba	**Sn**	**Fe**	**As**
18.2 ± 0.3	1.6 ± 0.2	41.5 ± 0.2	38.8 ± 0.2
BKFA-2-A			
#1 $\sim$ *(*$Ba_{0.59\pm0.06}K_{0.40\pm0.05}$*)*$Fe_{1.9\pm0.1}As_{1.9\pm0.1}$			
Ba	**K**	**Fe**	**As**
12.1 ± 0.5	8.4 ± 0.5	39.44 ± 0.08	39.9 ± 0.2
#2 $\sim (Ba_{0.81}K_{0.19})Fe_{2.1}As_{2.1}$ 2 points only			
15.7	3.6	40.2	40.5
BKFA-3-A $\sim (Ba_{0.75\pm0.03}K_{0.25\pm0.02})Fe_{2.02\pm0.06}As_{2.03\pm0.06}$			
Ba	**K**	**Fe**	**As**
14.8 ± 0.2	5.0 ± 0.3	40.0 ± 0.2	40.2 ± 0.2
BKFA-5-A			
#1 $\sim$ *(*$Ba_{0.74\pm0.03}K_{0.26\pm0.03}$*)*$Fe_{2.13\pm0.08}As_{2.13\pm0.09}$			
Ba	**K**	**Fe**	**As**
14.0 ± 0.2	5.0 ± 0.4	40.5 ± 0.2	40.5 ± 0.2
#2 $\sim (Ba_{0.16}K_{0.84})Fe_{1.9}As_{2.0}$ 2 points only			
3.3	17.0	39.2	40.5

Table 3.2: The EDS analysis for BKFA-6-A showing the atomic % of each element, the empirical chemical formula and all associated errors values. The associated errors were determined using the standard deviation from multiple EDS measurements points. The italic composition is the dominant composition for BKFA-6-A.

BKFA-6-A			
# 1 ~ $(Ba_{0.72\pm0.01}K_{0.280\pm0.008})Fe_{2.05\pm0.03}As_{2.04\pm0.03}$			
Ba	**K**	**Fe**	**As**
14.16 ± 0.07	5.5 ± 0.1	40.3 ± 0.2	40.1 ± 0.2
# 2 ~ $(Ba_{0.56\pm0.06}K_{0.44\pm0.04})Fe_{2.1\pm0.1}As_{2.0\pm0.1}$			
Ba	**K**	**Fe**	**As**
11.0 ± 0.6	8.7 ± 0.3	40.4 ± 0.1	39.9 ± 0.3
# 3 ~ $(Ba_{0.26\pm0.08}K_{0.7\pm0.1})Fe_{2.1\pm0.2}As_{2.2\pm0.1}$			
Ba	**K**	**Fe**	**As**
5 ± 1	14.2 ± 0.7	39.9 ± 0.3	40.9 ± 0.4
# 4 ~ $(Ba_{0.04\pm0.01}K_{0.96\pm0.05})Fe_{2.0\pm0.1}As_{2.0\pm0.1}$			
Ba	**K**	**Fe**	**As**
0.8 ± 0.2	19.21 ± 0.08	40.1 ± 0.2	40.0 ± 0.2

The presence of multiple compositions for BKFA-2-A, BKFA-5-A and BKFA-6-A were observed using EDS analysis. Two compositions were observed for BKFA-2-A and BKFA-5-A while four compositions were observed for BKFA-6-A[3]. Composition #1 for BKFA-2-A was close to its target compound while composition #2 was significantly different from its target composition. Compositions #1 and #2 for BKFA-5-A differed significantly from its target composition due to a furnace malfunction during the crystal growth. In BKFA-6-A, four compositions were found using EDS but only composition #3 corresponded to its target composition. The presence of multiple compositions for Sn single crystal growths of $(Ba_{1-x}K_x)Fe_2As_2$ has been observed by Ni *et al.*[5] and Johrendt *et al.*[17]. Ni *et al.*[5] concluded that the amount of potassium differed in the single crystals after measuring the resistivity of two single crystals of $(Ba_{0.55}K_{0.45})Fe_2As_2$[5]. Johrendt *et al.*[17] concluded that the single crystals were inhomogeneous due to the amount of potassium present in the flux changing as the crystals are grown[17].

The most interesting aspect of the EDS analysis was spontaneous stoichiometry changes observed in BKFA-6-A. When measuring the resistivity of BKFA-6-A, two superconducting transitions were observed for the single crystal. Subsequently, a scanning electron microscope (SEM) image of the single crystal was captured and two distinct phases of the single crystals were observed (see Figure 3.2). In Figure 3.2, two phases (#1 and #2) can clearly be seen in addition to the well defined separation between the two phases. EDS analysis was performed on another single crystal of BKFA-6-A showing two distinct phases (see Figure 3.3). EDS spectrum were obtained for the points along the 200 μm yellow line in Figure 3.3a). The results of the EDS scanning along the yellow line can be seen in Figure 3.3b). The amounts of Fe

[3]The target composition for each single crystal growth can be seen in Tables 2.1 while the EDS results for each growth can be seen in Table 3.1 and 3.2.

and As were observed to remain approximately constant while the amounts of Ba and K showed a distinct transition. The transition boundary between the two phases of the single crystal (i.e. at 50 μm in the Figure 3.3b) corresponded to the interchanging of potassium and barium concentrations. Phase #1 of the single crystal corresponds to composition #3 in Table 3.2 while phase #2 of the single crystal corresponds to composition #1 in Table 3.2. The presence of these two distinct phases implies that the addition of potassium as a dopant does not result in the two separate pure phases (KFe_2As_2 and $BaFe_2As_2$) but rather two mixed states with rational K to Ba ratios.

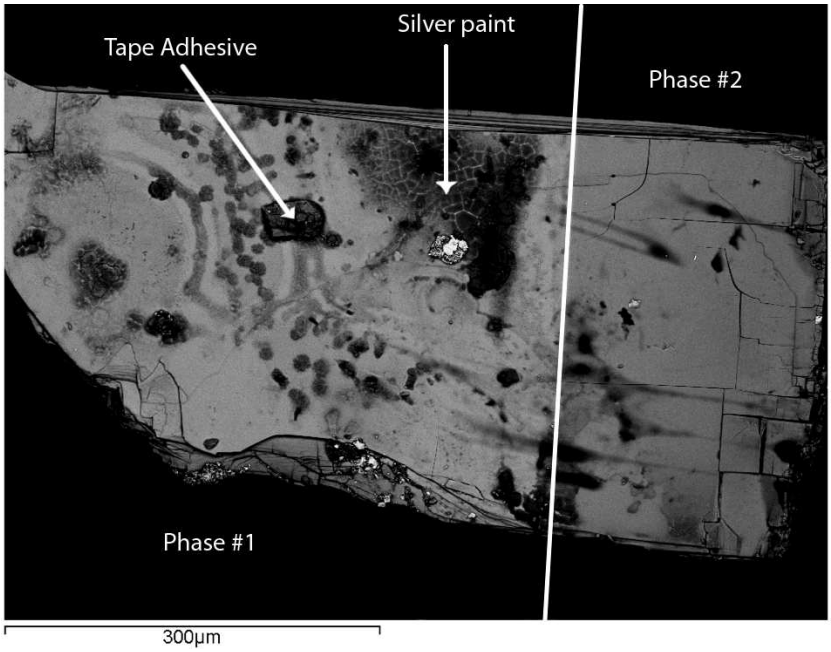

Figure 3.2: Scanning electron microscope image of BKFA-6-A showing two phases (#1 and #2) and the phase separation. The speckled area on the surface of the single crystal was caused by the silver paint and adhesive used in the resistivity measurements. The black background in the image is caused by the carbon tape used to attach the single crystal to the holder.

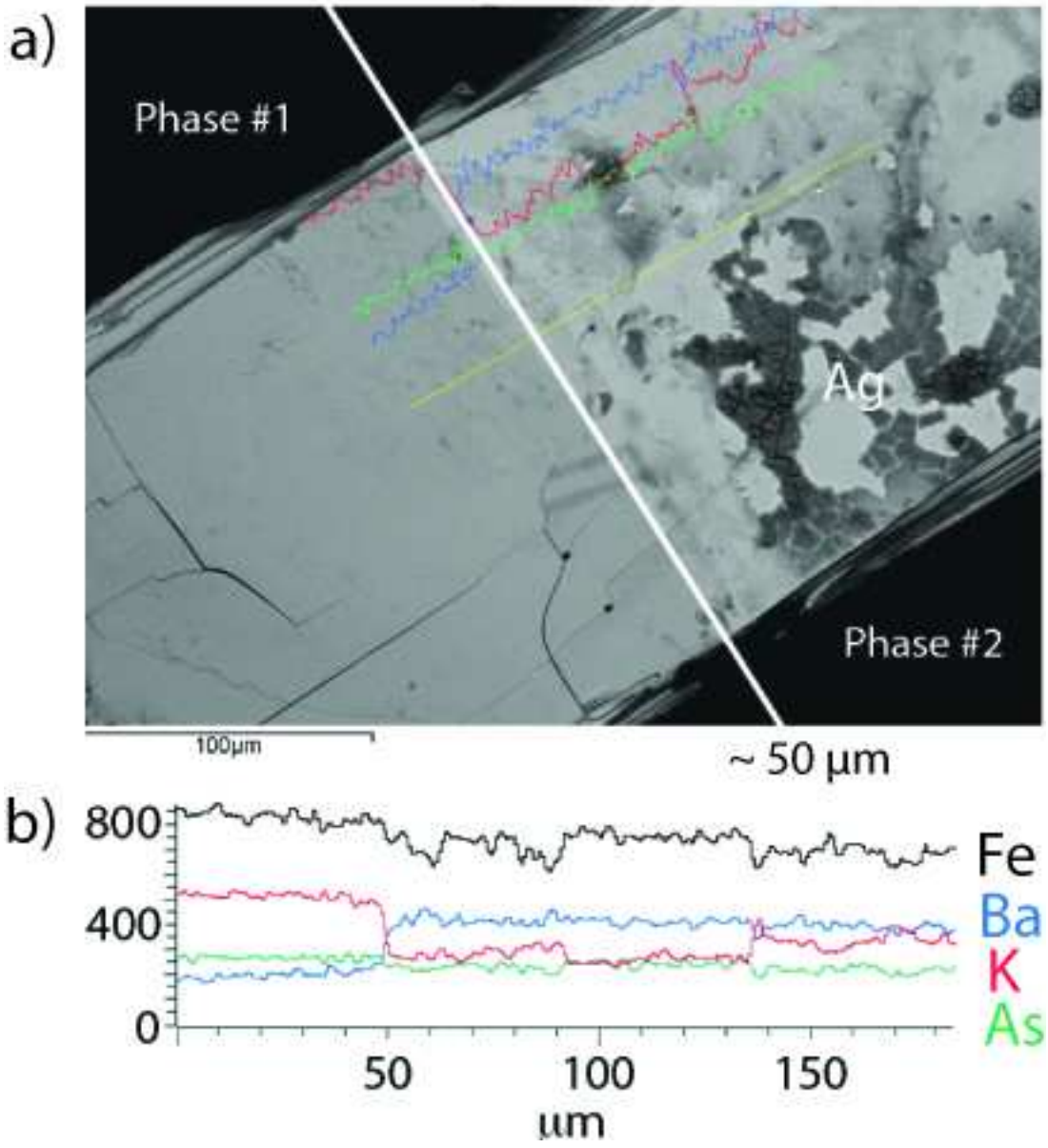

Figure 3.3: Scanning electron microscope image of BKFA-6-A showing two phases (#1 and #2) with the EDS analysis and the silver paint (Ag). The EDS analysis was performed along a straight yellow line in the image of BKFA-6-A. The black background in the SEM image is caused by the carbon tape used to attach the single crystal to the holder.

3.2 Single Crystal X-ray Diffraction

Single crystal X-ray diffraction was used as a tool to characterize and determine the lattice parameters of the single crystals. One single crystal from each batch was randomly selected for single crystal X-ray diffraction. The single crystal X-ray diffraction measurements were performed with a Stoe & Cie GmbH. IPDS2 single crystal X-ray diffractometer using graphite-monochromatized Mo Kα radiation ($\lambda = 0.71073$ Å). The diffractometer used a 340 mm imaging plate to record the X-ray photograph. The photographs of the single crystals were produced by rotating the single crystals in the X-ray beam using the precession method[4]. The photographs were then digitized using a laser and photomultiplier to obtain the relative intensity and absolute position of the spots on the plate. Each photograph is a flattened image of the diffraction sphere surface for a particular orientation of the single crystal. The spots observed in the photographs correspond to the lattice planes of a single crystal[50].

The crystal structure and lattice parameters were determined using the captured photographs. To obtain the lattice parameters of the single crystals, the photographs were analyzed using Stoe's X-Area detector software. Eighteen photographs were captured in different orientations in order to obtain an undistorted image of the diffraction sphere's surface[50]. When all eighteen photographs are compiled together, the detector software was used to determine the crystal structure and lattice parameters. The crystal structure of all single crystals was determined to be tetragonal I4/mmm with the lattice parameters presented in Table 3.3. The lattice parameters from literature for $(Ba_{1-x}K_x)Fe_2As_2$ can be seen in Table 3.4. The variation of the lattice parameters as a function of potassium concentration can also be seen in Figure 1.4.

[4]The precession method rotates the single crystal in the monochromatic X-ray beam to create an undistorted image of the diffraction sphere's surface. For more information on the precession method and single crystal XRD, see [50].

From Figure 1.4, it can clearly be seen that lattice parameter **a** should decrease while

Table 3.3: The lattice parameters (**a** and **c**) determined using the single crystal X-ray diffraction for single crystals from BKFA-1-NA to BKFA-6-A at 293 K.

Batch	**a**	**c**
BKFA-1-NA	3.94609(5) Å	13.1594(8) Å
BKFA-2-A	3.920(3) Å	13.29(7) Å
BKFA-3-A	3.932(1) Å	13.286(5) Å
BKFA-4-A	3.9301(7) Å	13.239(6) Å
BKFA-5-A	3.91(1) Å	13.40(1) Å
BKFA-6-A	3.902(5) Å	13.42(2) Å

lattice parameter **c** should increase as the concentration of potassium increases. In agreement, it was observed that the lattice parameter **a** decreased and **c** increased when potassium was present in the single crystals (see Table 3.3) . For example, the lattice parameter **a** was observed to decrease and **c** was observed to increase when BKFA-1-NA was compared to the other five batches. For BKFA-1-NA and BKFA-2-A, the lattice parameters **a** and **c** are comparable to the Ni *et al.*[5] results. For further comparison, the lattice parameters from literature were compiled in Table 3.4 and plotted in Figure 3.4. In Figure 3.4, it was observed that the lattice parameters of BKFA-1-NA, BKFA-2-A, BKFA-3-A and BKFA-6-A were close to the line of best fit while BKFA-5-A was significantly off the line of best fit. The variation and deviation from the line of best fit for the literature of the lattice parameters of the single crystals grown for this thesis are attributed to the inhomogeneous distribution of potassium in single crystal growth.

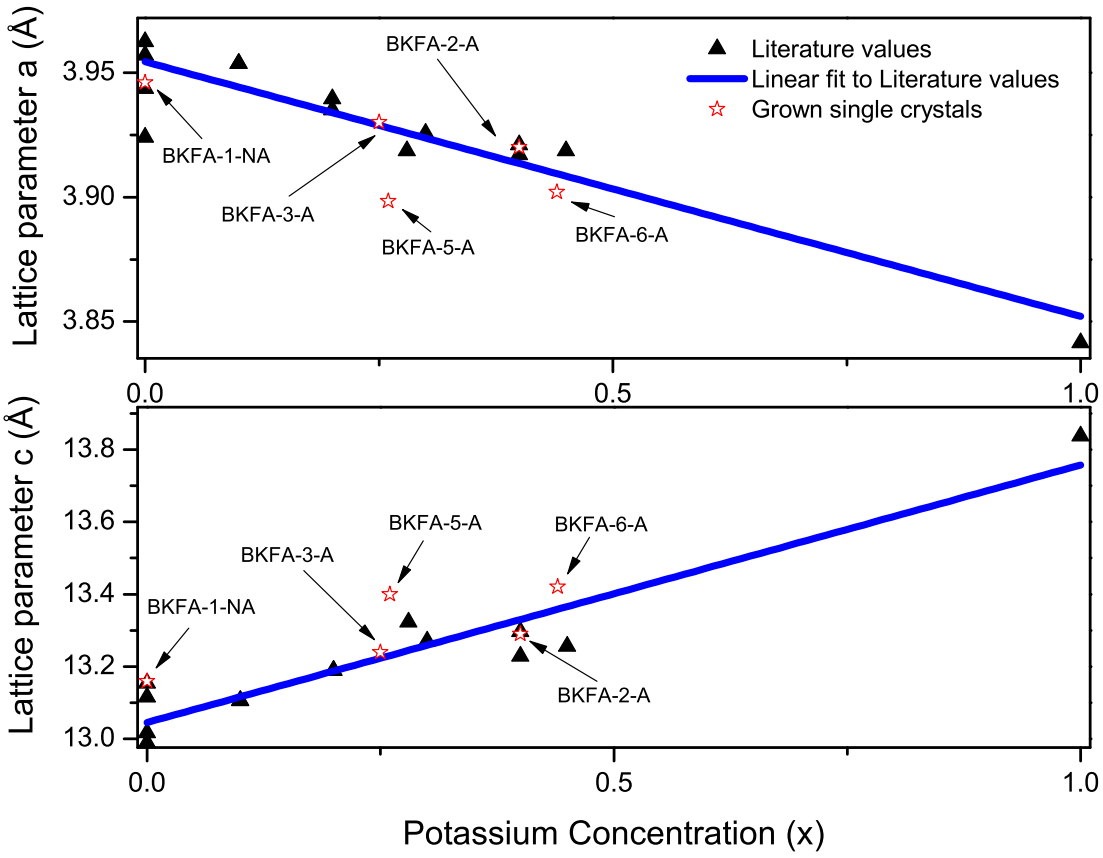

Figure 3.4: The dependence of the lattice parameters on the potassium concentration. The potassium concentrations for each pair of lattice parameters were determined using the EDS analysis and dominant compositions.

Table 3.4: The lattice parameters from literature for $(Ba_{1-x}K_x)Fe_2As_2$ with tetragonal I4/mmm crystal structure. The lattice parameters were all measured at room temperature.

Compound	**Method**	**a**	**c**	**Reference**
$BaFe_2As_2$	FeAs flux	3.9241 Å	13.1536Å	Sun *et al.*[22]
$BaFe_2As_2$	Polycrystalline	3.9625(1)Å	13.0168(3) Å	Rotter *et al.*[18]
$BaFe_2As_2$	Polycrystalline	3.957Å	12.989 Å	Wu *et al.*[20]
$BaFe_2As_2$	Sn flux	3.9436 Å	13.115 Å	Ni *et al.*[5]
$Ba_{0.9}K_{0.1}Fe_2As_2$	Polycrystalline	3.9537(1) Å	13.1060(1) Å	Rotter *et al.*[51]
$Ba_{0.8}K_{0.2}Fe_2As_2$	Polycrystalline	3.9395(1) Å	13.1890(1) Å	Rotter *et al.*[51]
$Ba_{0.72}K_{0.28}Fe_2As_2$	FeAs flux	3.9186 Å	13.3227 Å	Sun *et al.*[22]
$Ba_{0.7}K_{0.3}Fe_2As_2$	Polycrystalline	3.9257(1) Å	13.2702(3) Å	Rotter *et al.*[51]
$Ba_{0.6}K_{0.4}Fe_2As_2$	Polycrystalline	3.921 Å	13.228 Å	Wu *et al.*[20]
$Ba_{0.6}K_{0.4}Fe_2As_2$	Polycrystalline	3.9170(1) Å	13.2968(1) Å	Rotter *et al.*[3]
$Ba_{0.55}K_{0.45}Fe_2As_2$	Sn flux	3.9186 Å	13.256 Å	Ni *et al.*[5]
KFe_2As_2	Polycrystalline	3.8414(2)Å	13.837(1) Å	Sasmal *et al.*[8]

3.3 Magnetic Measurements

Magnetic properties of the single crystals were measured using a Quantum Design MPMS-XL 5 D.C. SQUID[5]. Single crystals were randomly chosen from each batch for the magnetic measurements. When measuring the temperature dependent or field dependent magnetization, the samples were mounted on a clear/white plastic straw using a small amount of silicon grease or gel capsule. When measuring the effect of annealing on the temperature dependent magnetization, the sample was sealed in a helium filled high purity quartz tube.

3.3.1 Temperature Dependent Magnetic Measurements

Anisotropic Magnetization of $BaFe_2As_2$

The anisotropic magnetization for $BaFe_2As_2$ was measured using a single crystal from BKFA-1-NA. The mass magnetization[6]for a single crystal of BKFA-1-NA was measured using a magnetic field of 20000 G in both the in-plane and out of plane orientation. The resulting curves can be seen in Figure 3.5 while the Ni *et al.*[5] measurements for $BaFe_2As_2$ can be seen in Figure 1.10 (p. 15). In Figure 3.5, it can clearly be seen that both curves are paramagnetic with no superconducting transition present. When comparing the results of Ni *et al.*[5] to Figure 3.5, it is observed that the in-plane curve shifted away from the out of plane curves at low temperature in both figures. The shifting of the in-plane curve at low temperature was attributed to the orthorhombic distortion transition and the strong anisotropic effects. In Figure 3.5, it was also observed that the out of plane curve shifts away from the in-plane

[5]For a detailed explanation of how SQUIDs function and underlying quantum mechanics, please see the additional references in Appendix A.

[6]The mass magnetization is calculated by dividing the magnetic moment (in emus) of the sample by the mass of the sample (in grams).

curve above 100 K while in Figure 1.10 the in-plane and out of plane curves coincide. It is important to note that different units are used in both figures. But the use of different units does not account for the shifting of the out of plane curve away from the in-plane curve. Thus the cause of the high temperature shifting is unknown.

To further analyze the magnetization of BFKA-1-NA, the in-plane magnetization seen in Figure 3.5 was converted from mass magnetization to molar susceptibility in order to compare with the Ni *et al.*[5] results (see Figure 3.6). Ni *et al.*[5] observed that two Curie-Weiss[7] curves could be fitted to the in-plane molar susceptibility with the intersection of the two curves occurring near the orthorhombic transition temperature (∼85 K). It was found that the effective moment was similar for the Curie-Weiss fitting curves while the temperature parameter was observed to be positive above the transition and negative below the transition. For BKFA-1-NA, two Curie-Weiss curves were fitted to the in-plane molar susceptibility of BKFA-1-NA and the results are presented in Figure 3.7. The two Curie-Weiss curves were observed to intersect at 84(1) K while the temperature parameters were -2.983 K and 29.866 K below and above the transition, respectively. The effective moment for both Curie-Weiss fits were different with both being less than the Ni *et al.*[5] values. The variation and overall difference relative to the Ni *et al.*[5] results were attributed to the presence of a very small amount of potassium in the BKFA-1-NA single crystals.

[7]Curie-Weiss paramagnetism occurs when the magnetic moments interact with each other resulting in the addition of the temperature parameter to the Curie's law. Curie-Weiss law states that: $\chi = \frac{C}{T-\theta}$ where C is the Curie constant and θ is the temperature parameter[52]. For a more detailed explanation of Curie-Weiss paramagnetism and Curie's law, see Chapter 9 of [52].

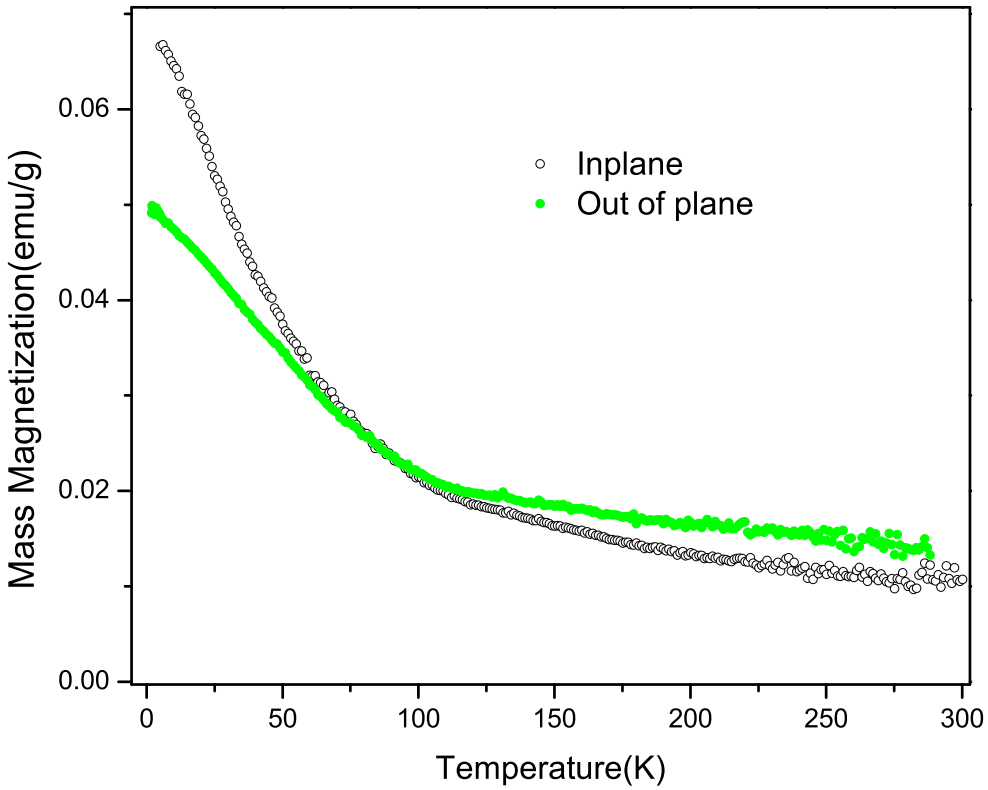

Figure 3.5: Anisotropic mass magnetization of BKFA-1-NA showing the in-plane and out of plane curves with H = 15000 G.

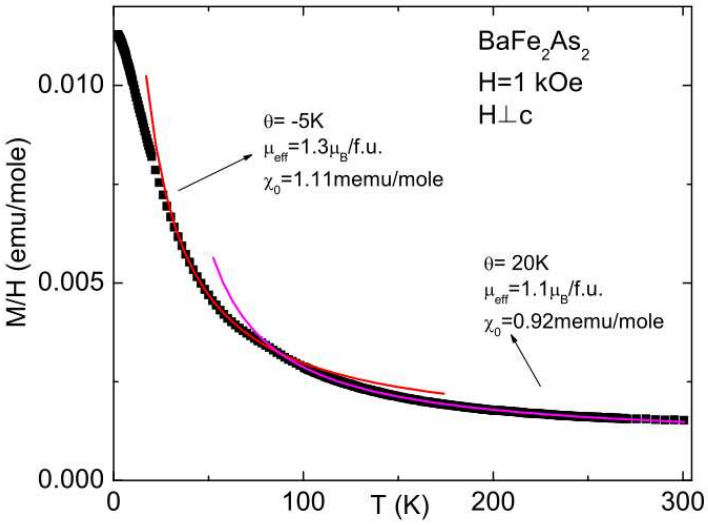

Figure 3.6: The in-plane molar magnetization of $BaFe_2As_2$ with two Curie-Weiss fits. Reprinted from [5].

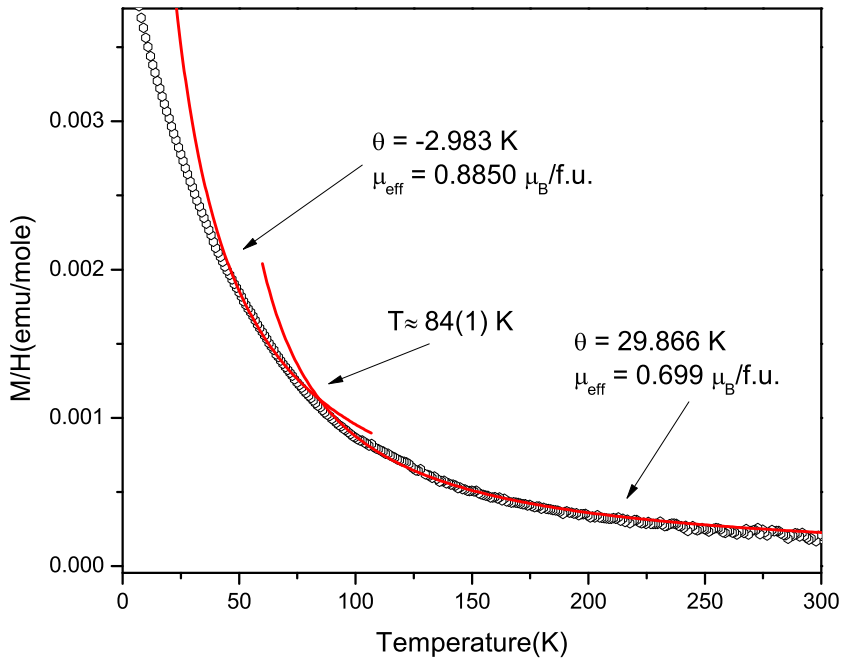

Figure 3.7: The in-plane molar magnetization of BKFA-1-NA with two Curie-Weiss fits. The two Curie-Weiss fittings are observed to intersect at 84(1) K.

Superconducting Phase of $(Ba_{1-x}K_x)Fe_2As_2$

The superconducting phase of the grown single crystals was investigated using low field temperature dependent magnetization measurements. The temperature dependent in-plane magnetization for the grown single crystals can be seen in Figures 3.8 to 3.12. Using the magnetization curves for the grown single crystals, the onset transition temperatures were determined by extrapolating the magnetization curve. The superconducting transition temperatures for the grown single crystals are seen in Table 3.5. where it can clearly be seen that all single crystal batches except for

Table 3.5: The superconducting transition temperatures for BKFA-1-NA to BKFA-6-A determined using temperature dependent magnetization. Each transition temperature in the table corresponds to different single crystals.

Batch	**Onset Transition Temperatures, T_c**
BKFA-1-NA	No superconducting transition was observed.
BKFA-2-A	37.03 K and 36.75 K
BKFA-3-A	36.60 K, 36.30 K, 37.73 K, 35.50 K and 37.84 K
BKFA-4-A	36.80 K, 37.29 K; 27.9 K; 16.0 K
BKFA-5-A	18.2 K; 25.00 K; 35.60 K
BKFA-6-A	26.96 K and 26.65 K

BKFA-1-NA were superconducting with onset superconducting transition temperatures ranging from 16.0 K to 37.14 K.

The results from Table 3.5 were then compared to the EDS results in Table 3.1 and the Ni *et al.*[5] results. It was found that the number of phases for each batch varied in Table 3.1 and Table 3.5. For BKFA-2-A, two phases were found using EDS

while only one phase was found using magnetization measurements. For BKFA-4-A, one phase was found using EDS while three phases were found using the magnetization measurements. For BKFA-5-A, two phases were found using EDS while three phases were found using magnetization measurements. For BKFA-6-A, four phases were found using EDS while one phase was found using magnetization measurements. The differing number of phases found for each batch was attributed to the variation of potassium in the single crystal batches. The mass magnetization curves for the single crystals were then compared to the Ni *et al.*[5] results. It was observed that the mass magnetization of BKFA-2-A and BKFA-4-A were comparable to the Ni *et al.*[5] results albeit the onset superconducting transition temperatures were higher than Ni *et al.*[5] observed. The mass magnetization of BKFA-3-A, BKFA-5-A and BKFA-6-A were not comparable to the Ni *et al.*[5] results. It was observed that the results were not comparable due to the shallow slope of the magnetization curves below the T_c.

The source of the shallow slope in the magnetization curves could be the presence of the multiple phases observed in section 3.1 using EDS/SEM. The presence of the multiple phases would affect the magnetic properties as follows: the dominant phase of the single crystal would have the highest T_c and the secondary phases could be paramagnetic or superconducting with a lower T_c than the dominant phase. The magnetic properties of the secondary phases are completely dependent on the localized potassium concentration. If the secondary phase phases were primarily paramagnetic (i.e. $x < 0.1$), the magnetization would not be affected by the secondary phases due to the weak magnitude of the applied magnetic field. If the secondary phase were primarily superconducting (i.e $x > 0.1$), the diamagnetic signal of the dominant phase below superconducting transition temperatures of the secondary phases would be increased. Above the superconducting transition temperatures of the secondary phases, the secondary phases would become paramagnetic again. Overall the

dominant superconducting transition would be marginal to poor, since weak superconducting secondary phases would prevent the diamagnetic signal from decreasing quickly with respect to temperature and broaden the superconducting transition.

The presence of multiple phases in the grown single crystals were then analyzed using low field temperature dependent magnetization measurements. For BKFA-2-A, BKFA-3-A, and BKFA-4-A, it was observed that a second transition in the zero field cool curve was observed between 12 K and 16 K. It was also observed that the magnetization decreased quickly after the dominant T_c and then slowly decreased linearly. In BKFA-3-A, the dominant superconducting transition temperatures for the three single crystals were equal but the overall shape of the curves varied due to bulk superconducting volume of the single crystals differing. Thus it was concluded that BKFA-2-A, BKFA-3-A(crystal 1 and 2) and BKFA-4-A had at least one secondary superconducting phase. For BKFA-3-A(crystal 3), it was observed that the diamagnetic signal decreased linearly with a broad hump near 16 K due to secondary phases. For BKFA-5-A and BKFA-6-A, multiple phases caused the slow decrease in the diamagnetic signal. It was concluded that the presence of the multiple phases significantly effects the magnetization of BKFA-5-A and BKFA-6-A. Hence it was concluded that secondary phases were present in all single crystals batches. Overall, the effect of the secondary phases of magnetization as discussed in the previous paragraph was in agreement with the magnetization measurements. Furthermore, the presence of secondary phases and spontaneous stoichiometric changes observed using SEM are both caused by the nucleation of the single crystals during the crystal growth. Thus it was concluded that the secondary phases are a unique characteristic property of the single crystals grown using the Sn flux method.

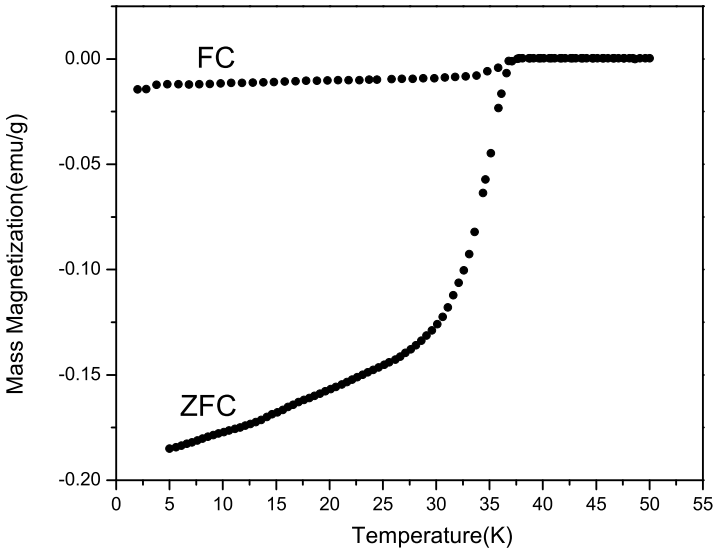

Figure 3.8: In-plane mass magnetization of BKFA-2-A for H = 10 G showing the zero field cool (ZFC) and field cool (FC) curves.

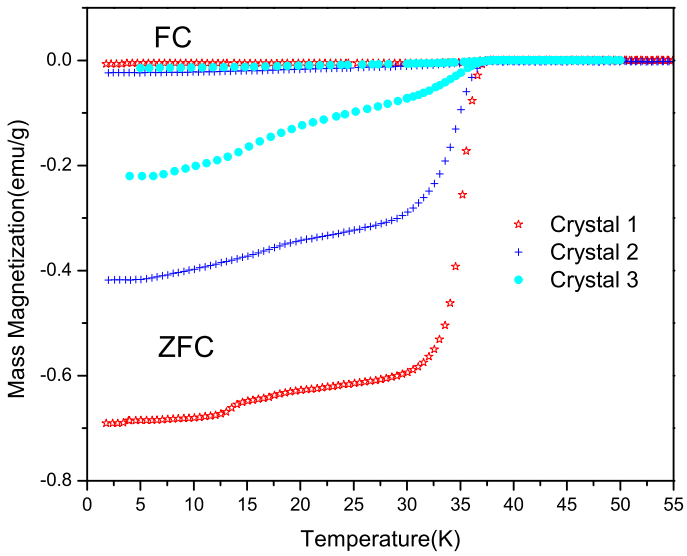

Figure 3.9: In-plane mass magnetization of BKFA-3-A for H = 10 G showing the zero field cool curves of three different single crystals.

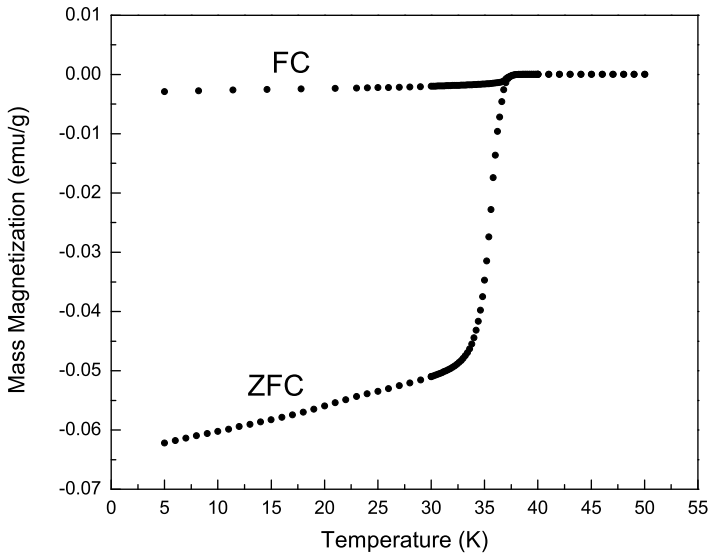

Figure 3.10: In-plane mass magnetization of BKFA-4-A for H = 10 G showing the zero field cool (ZFC) and field cool (FC) curves.

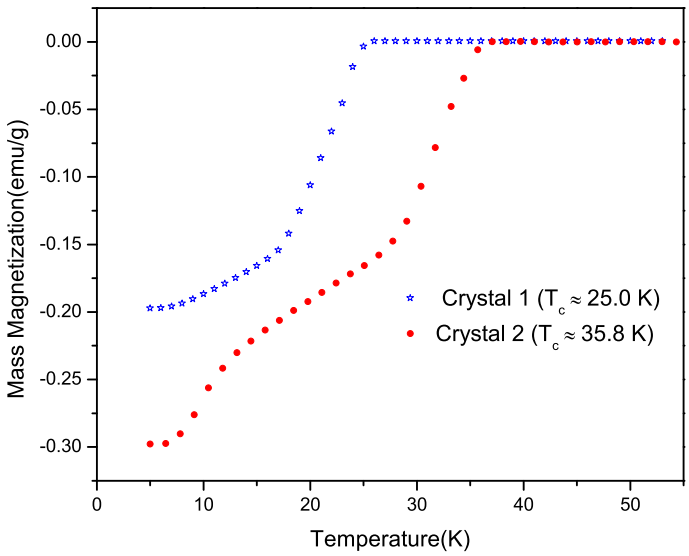

Figure 3.11: In-plane mass magnetization of BKFA-5-A for H = 10 G showing the zero field cool curves of two different single crystals.

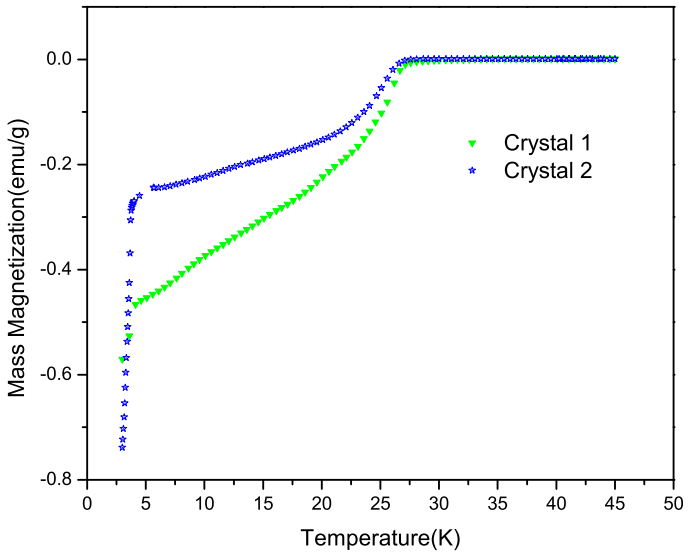

Figure 3.12: In-plane mass magnetization of BKFA-6-A for H = 10 G showing the zero field cool curves of two different single crystals. The superconducting transition around 3.6 K is due to the presence of Sn in the single crystals.

Paramagnetic Phase of $(Ba_{1-x}K_x)Fe_2As_2$

The paramagnetic phase of $(Ba_{1-x}K_x)Fe_2As_2$ was investigated using high field temperature dependent magnetization measurements. The paramagnetic phases of BKFA-4-A and BKFA-5-A were examined using a magnetic field of 15000 G for temperatures from 5 K to 300 K. The paramagnetic temperature dependent magnetization for BKFA-4-A and BKFA-5-A can be seen in Figures 3.14 and 3.15, respectively. In Figures 3.14 and 3.15, paramagnetic behavior is observed above the superconducting transition with diamagnetic behavior below the T_c. The superconducting transition temperatures for the single crystals of BKFA-4-A and BKFA-5-A were then determined from the low temperature proportion of the the magnetization curves. The superconducting transition temperature for BKFA-4-A and BKFA-5-A were 27.9 K and 18.2 K respectively.

The presence of the additional transition (T_*) near 85 K can also be seen in Figures 3.14 and 3.15. Ni *et al.*[5] performed similar measurements on Sn flux single crystals of $(Ba_{0.55}K_{0.45})Fe_2As_2$ and $BaFe_2As_2$ (see Figure 3.13). In Figure 3.13, the in-plane molar susceptibility of $BaFe_2As_2$ has a small kink in the curve near 85 K due to the orthorhombic distortion transition. Furthermore, the in-plane molar susceptibility of $(Ba_{0.55}K_{0.45})Fe_2As_2$ displays no transition near 85 K since the orthorhombic distortion transition is suppressed by potassium doping. In the case of polycrystalline and self flux single crystals, the orthorhombic and SDW transition is completely suppressed for $x > 0.3$. But in the case of Sn flux single crystals, the SDW transitions may be suppressed/masked by the incorporation of Sn into the crystal structure, and hence only the orthorhombic distortion transition will be observed. Using the superconducting transition temperatures from Figures 3.14 and 3.15, it was found that the potassium concentration in the single crystals were approximately 0.20 and 0.15, respectively[8]. Since the orthorhombic distortion transition was observed for both BKFA-4-A and BKFA-5-A, it can be concluded that the orthorhombic distortion transition is present for $x \leq 0.20$. No systematic study of Sn flux single crystals has been performed hence the amount of potassium required for complete suppression of the orthorhombic distortion transition is not known.

[8]The concentrations of potassium were approximated using the superconducting transition temperatures and Figure 1.5 on p. 7.

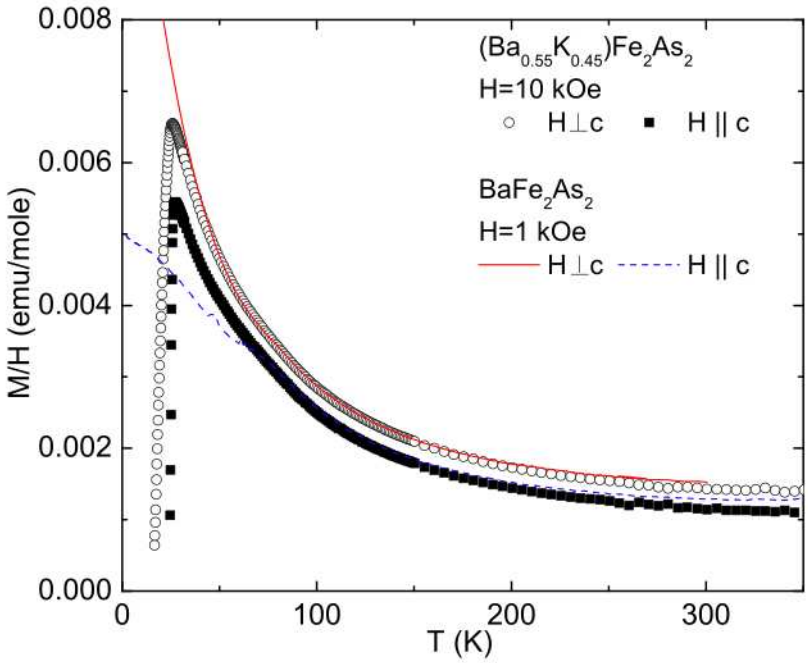

Figure 3.13: In-plane and out of plane temperature dependent molar susceptibility for $(Ba_{0.55}K_{0.45})Fe_2As_2$ and $BaFe_2As_2$. Reprinted from [5].

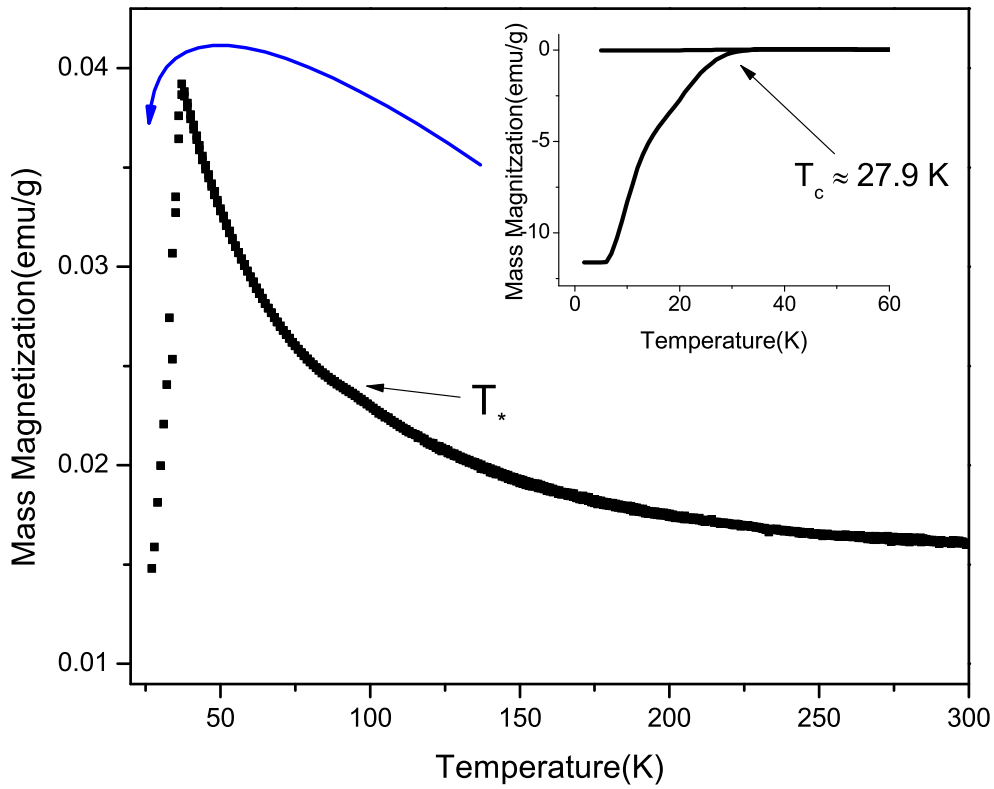

Figure 3.14: In-plane temperature dependent high field magnetization measurement for BKFA-4-A. Inset: The low temperature portion of the in-plane magnetization curve showing the superconducting transition. A magnetic field of 5000 G was used for this measurement.

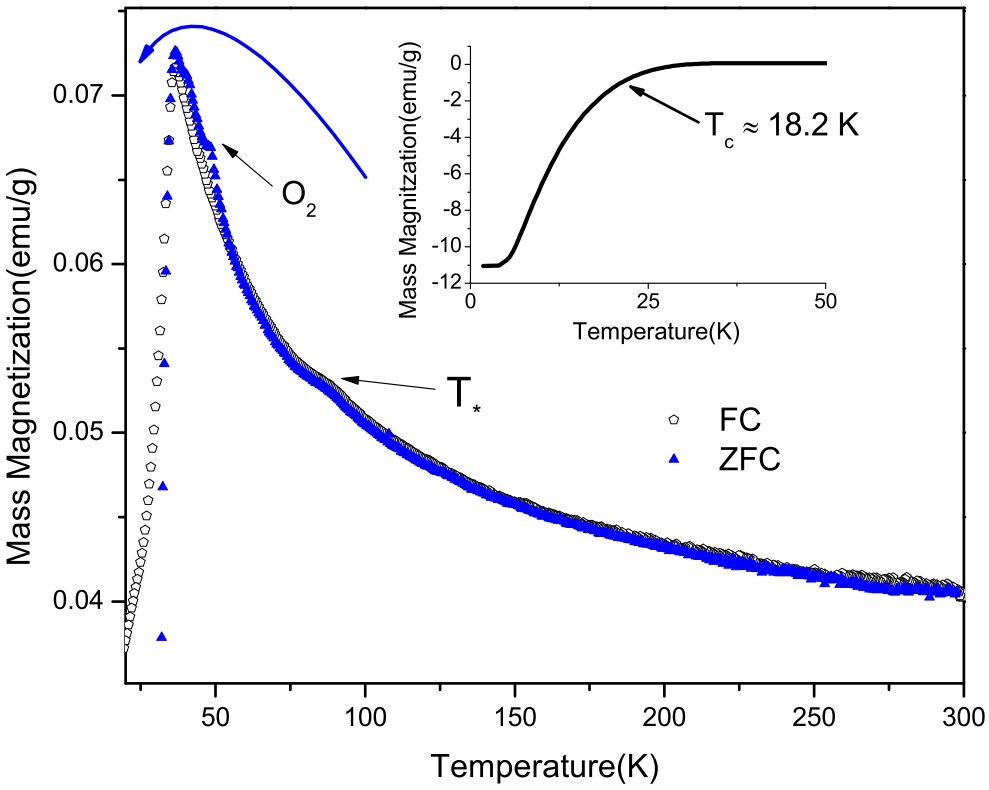

Figure 3.15: In-plane high field magnetization measurement for BKFA-5-A. The presence of oxygen contamination can be seen in the zero field cool (ZFC) curve. Inset: The low temperature portion of the in-plane magnetization curve showing the superconducting transition. A magnetic field of 5000 G was used for this measurement.

3.3.2 Field Dependent Magnetization Measurements

The paramagnetic phase of $(Ba_{1-x}K_x)Fe_2As_2$ was further investigated using field dependent in-plane magnetization measurements. The effect of the orthorhombic distortion transition on the field dependent magnetization is examined by measuring the magnetization above and below this transition. The field dependent magnetization measurements were performed on the single crystals at two temperatures: 50 K and 110 K. The paramagnetic phase of four crystal batches was examined: one crystal from BKFA-1-NA, BKFA-3-A, and BKFA-5-A and two single crystals from BKFA-4-A[9] The in-plane field dependent magnetization measurements are presented in Figures 3.16 to 3.20. The temperature dependent magnetization curves for the measured single crystals are inset into each figure.

The most striking feature of the field dependent in-plane magnetization measurements was the presence of a magnetic anomaly below 5000 Gauss. The weakest magnetic anomaly was observed for BKFA-1-NA while the strongest magnetic anomaly was observed for BKFA-4-A. It was also observed that the strength of the magnetic anomaly was not affected by the orthorhombic distortion transition. From the magnetization of BKFA-4-A (see Figure 3.18) and BKFA-5-A (see Figure 3.20), it can clearly be seen that the presence of multiple phases does not affect the strength of the magnetic anomaly. From Figures 3.17, 3.18, and 3.20, it can be seen that the three different single crystals from different batches with similar T_c have magnetic anomalies with completely arbitrary strength. From Figures 3.18 and 3.19, it can be seen that two different single crystals from the same batch (BKFA-4-A) shows magnetic anomalies with different strengths (one weak and the other extremely strong). Since the strength of the magnetic anomaly displays completely arbitrary strength, it can be concluded that the magnetic anomaly is due to a magnetic impurity.

[9]The two single crystals are denoted using a and b.

The source of the magnetic impurities observed in the field dependent magnetization measurements is due an excess amount of elements or compounds from the single crystal growth. Since the magnetic impurity is observed for low fields, it can concluded that diamagnetic and paramagnetic elements could not produce the nonlinearity at low fields. All the elements in $(Ba_{1-x}K_x)Fe_2As_2$ except for Fe are paramagnetic or diamagnetic. Thus the excess element which produces the observed arbitrary magnetic impurity could be iron. Since iron powder was used in the Sn flux method, it is also possible that Fe_3O_4 was present in the Fe powder. Thus it is concluded that an excess amount of iron and/or iron(II,III) oxide could produce the observed magnetic impurity.

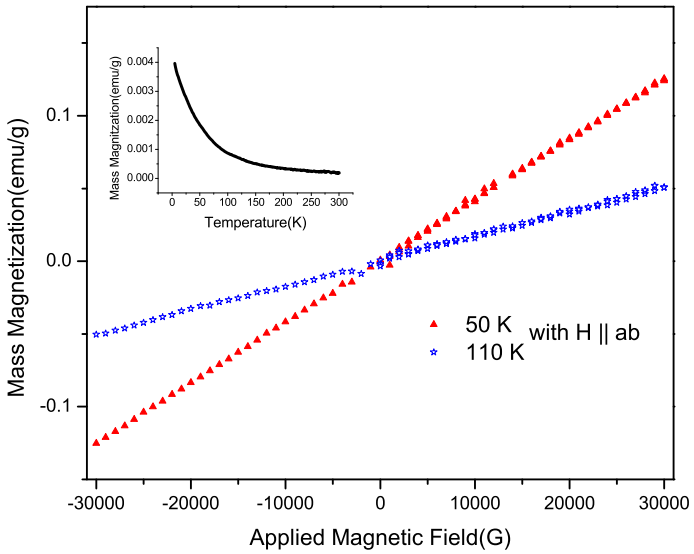

Figure 3.16: In-plane field dependent magnetization of BKFA-1-NA for T = 50 K and 110 K. Inset: The in-plane temperature dependent magnetization for the BKFA-1-NA with H = 7500 Gauss.

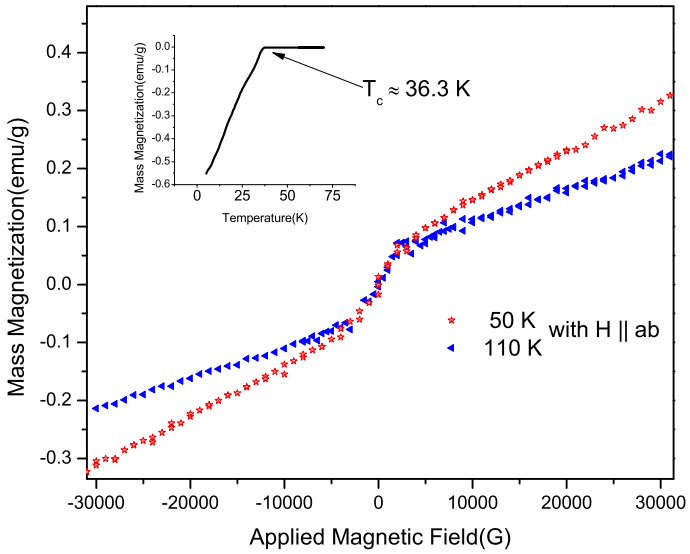

Figure 3.17: In-plane field dependent magnetization of BKFA-3-A for T = 50 K and 110 K. Inset: The in-plane temperature dependent magnetization for the BKFA-3-A with H = 30 Gauss.

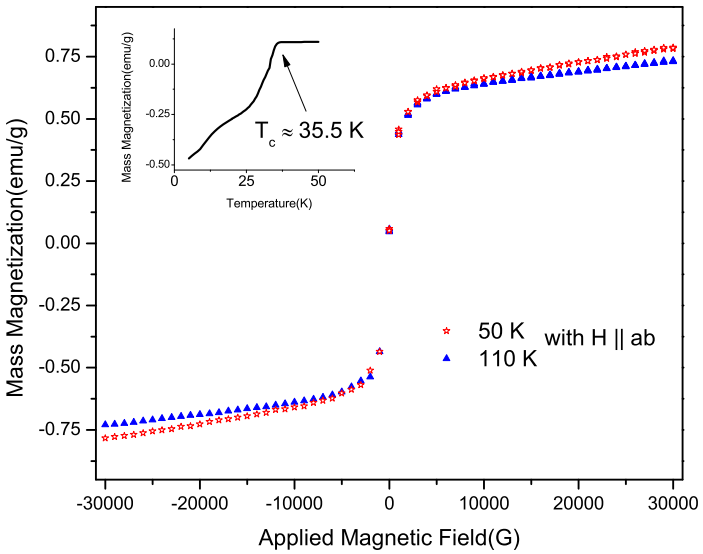

Figure 3.18: In-plane field dependent magnetization of BKFA-4-Aa for T = 50 K and 110 K. Inset: The in-plane temperature dependent magnetization for the BKFA-4-Aa with H = 30 Gauss.

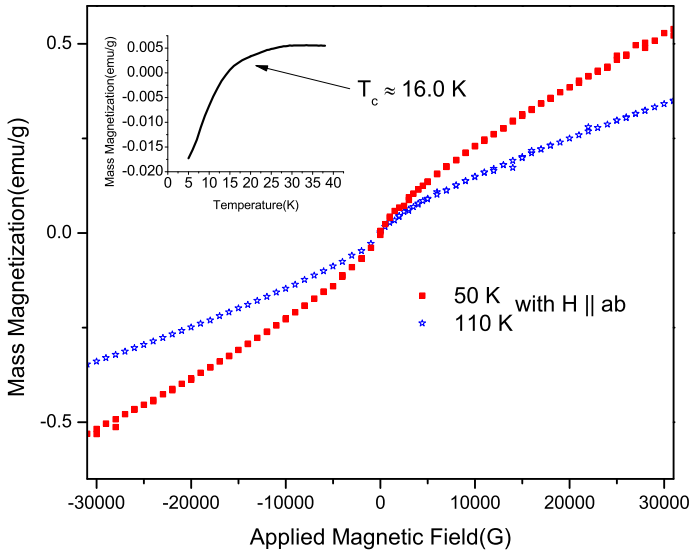

Figure 3.19: In-plane field dependent magnetization of BKFA-4-Ab for T = 50 K and 110 K. Inset: The in-plane temperature dependent magnetization for the BKFA-4-Ab with H = 100 Gauss.

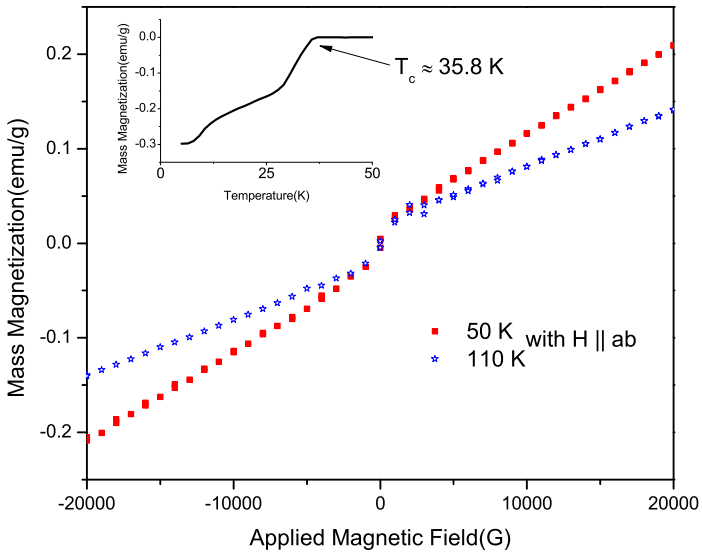

Figure 3.20: In-plane field dependent magnetization of BKFA-5-A for T = 50 K and 110 K. Inset: The in-plane temperature dependent magnetization for the BKFA-5-A with H = 100 Gauss.

3.3.3 The Effect of Annealing on the Magnetization Measurements

When using the Sn flux method to grow single crystals, it is important to understand the effect of the decantation on the single crystals. Since the single crystals were decanted at 500^{o}C, a significant amount of stress was induced in the single crystals. To remove stress induced in the single crystals during decantation, the annealing method was proposed. To determine the effect of annealing on the superconductivity properties of the single crystals, temperature dependent magnetization measurements were performed. The single crystals were first sealed in a high purity thin quartz tube with 1/3 atm. of helium. The 'as grown' magnetization curve was measured with the single crystal sealed in the quartz using heat shrink to secure the quartz tube to the transport rod. After the completion of the measurement, the single crystal sealed in the quartz tube was placed in a furnace and heated to a certain temperature for a specific time. When the heating time elapsed, the single crystal was removed from the furnace. The magnetic curve of the single crystal was then measured again under the same conditions.

The effect of annealing on the magnetic measurements was studied for BKFA-3-A. One single crystal from BKFA-3-A was sealed in a high purity thin quartz tube with 1/3 atm. of helium. For the BKFA-3-A, the single crystal was annealed twice: first at 200^{o}C for five hours and secondly at 250^{o}C for another five hours. The normalized magnetic susceptibility for BKFA-3-A is presented as Figure 3.21. It was observed that diamagnetic flux expulsion increased by a factor of $\sim$5 for BKFA-3-A after annealing the single crystals at 200^{o}C for five hours. The observed increase in the diamagnetic flux expulsion was attributed to the homogeneity of Ba/K distribution in the crystal structure increasing. Moreover, the increased homogeneity

of Ba/K distribution reduces the stress/strain induced during the rapid cooling and decantation. After the single crystal was annealed a second time, it was also observed that the diamagnetic flux expulsion decreased for the single crystal. Overall, the loss of the diamagnetic flux expulsion for the second annealing of the single crystal was likely caused by the loss of potassium and a resulting change in the stoichiometry of the crystals.

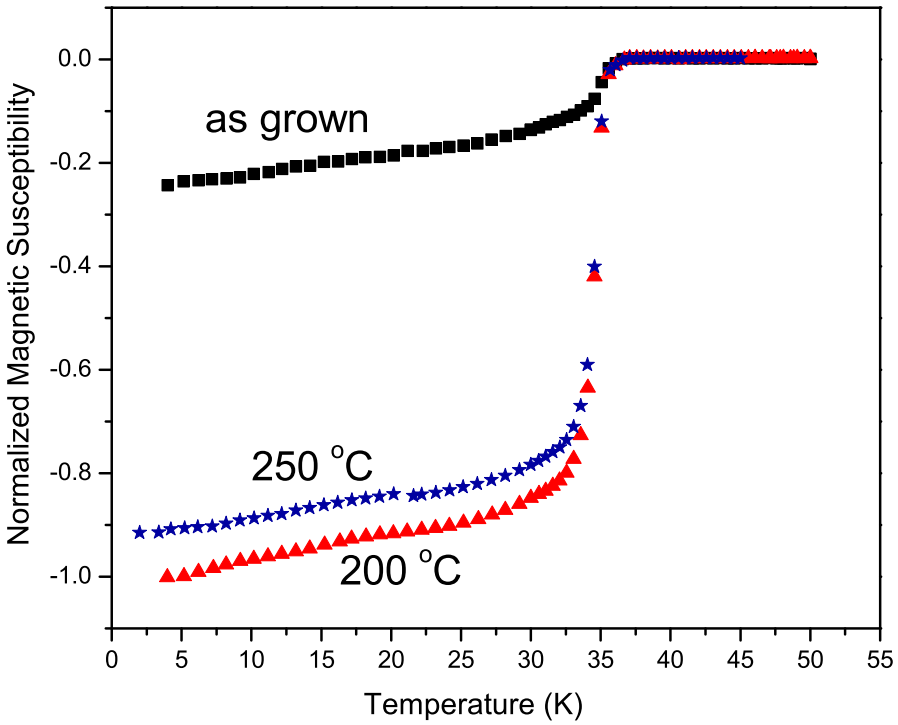

Figure 3.21: The effect of annealing on the temperature dependent in-plane magnetization for BKFA-3-A. The single crystal was annealed 200^{o}C for five hours and then at 250^{o}C for another five hours. The normalized magnetic susceptibility was calculated by dividing each curve by the 200^{o}C magnetization at 5 K.

3.4 Resistivity Measurements

The electrical properties of the single crystals prepared for this thesis were measured using a d.c. current source, a signal router, and a d.c. nanovoltmeter. The resistivity measurement were performed on randomly selected single crystals from each batch. To measure the temperature dependent resistivity for the grown single crystals, a Quantum Design MPMS-XL 5 D.C. SQUID with external device control or a cryostat were used to reach low temperature. To prepare the single crystals for the resistivity measurements, four thin gold wires were connected to the surface of a single crystal using either silver paint or silver paste. The gold wires were then connected to the measurement system using a microtip soldering iron and lead/tin solder.

3.4.1 Temperature Dependent Resistivity Measurements

Temperature dependent in-plane resistivity measurements were performed on the single crystals using the van der Pauw method[53]. The in-plane resistivity curves for BKFA-1-NA to BKFA-6-A can be seen in Figures 3.24 to 3.32. In Figures 3.24 to 3.32, it can be observed that the resistivity of the single crystals varied from 10^{-5} to 10^{-3} Ω·cm. The variation in the resistivity was attributed to cracks and defects in the single crystals. The superconducting transition temperatures for the single crystals were then determined using the middle point of the superconducting transition. The superconducting transition temperatures for the single crystals can be seen in Table 3.6. In Table 3.6, it can be observed that all single crystal batches except for BKFA-1-NA were superconducting. It can be seen that the superconducting transition temperatures range from 8.7 K to 36.5 K. It was also observed that multiple phases were present for BKFA-2-A and BKFA-6-A. For BKFA-2-A, it was found that

Table 3.6: The superconducting transition temperatures for BKFA-1-NA to BKFA-6-A determined using temperature dependent in-plane resistivity.

Batch	**Superconducting Transition Temperature, T_c**
BKFA-1-NA	No superconducting transitions were observed.
BKFA-2-A	32.0 K and 24.9 K
BKFA-3-A	36.5 K
BKFA-4-A	36.4 K
BKFA-5-A	17.4 K
BKFA-6-A	26.7 K, 26.2 K and 8.7 K

both phases significantly differed from the superconducting transition temperatures observed using the magnetization measurements (see Table 3.5 on p. 60). For BKFA-6-A, it was observed that one phase (26.7 K and 26.2 K) was comparable with the results in Table 3.5 while the second phase (8.7 K) was not comparable to Table 3.5. The superconducting transition temperatures for BKFA-1-NA, BKFA-3-A, BKFA-4-A and BKFA-5-A are comparable to those found in Table 3.5.

The resistivity curve for a nonsuperconducting BKFA-1-NA single crystal was examined to determine if the low temperature semiconducting behavior was observed. For BKFA-1-NA (see Figure 3.24), metallic behavior was observed from 85 to 300 K. Near 85 K, it was observed that the resistivity increased abruptly with decreasing temperature, followed by a slight decrease with decreasing temperature near 19 K. Some anomalous behavior occurred near 19 K which maybe due to small fractions of superconductivity in the crystal. The resistivity curve for BKFA-1-NA was then compared to the Ni *et al.*[5] resistivity curve for $BaFe_2As_2$ (see Figure 3.23). In Figure 3.23, it can be observed that the resistivity curve is metallic above 80 K followed

by semiconductor/semimetal behavior below 80 K with an abrupt increase in the resistivity at 80 K. Sun *et al.*[22] also observed similar behavior for Sn flux $BaFe_2As_2$ single crystals. It can be seen that Figure 3.24 and Figure 3.23 exhibit similar behavior, the difference being attributed to the presence of a small amount potassium in the single crystals of BKFA-1-NA.

The superconductivity for the doped single crystals was analyzed using the resistivity curves. The resistivity curves for the doped single crystals displayed metallic behavior above the superconducting transition. For BKFA-2-Aa and BKFA-3-A, it was observed that the the resistivity curves increased linearly with increasing temperature while the other resistivity curves were observed to increase logarithmically. The logarithmic increase in resistivity with increasing temperature has been seen for Sn flux single crystals, self flux single crystals and polycrystalline $(Ba_{1-x}K_x)Fe_2As_2$. The logarithmic increase of the resistivity implies that the resistivity is saturated[54], but the exact cause remains unclear. All of the doped single crystals had superconducting transitions between 8.7 K to 36.5 K.

The most striking feature of the resistivity curves was an increase in resistivity with decreasing temperature near ∼85 K. The increase in resistivity was observed for BKFA-2-Aa, BKFA-3-A and BKFA-4-A. Ni *et al.*[5] observed a similar increase for Sn flux $(Ba_{0.55}K_{0.45})Fe_2As_2$ (see Figure 3.22). Ni *et al.*[5] attributed the increase in the resistivity to the inhomogeneous arrangement of potassium in the layers of the single crystals or the variation of potassium concentration for different single crystals. The increase in the resistivity curve is not unique to Sn flux $(Ba_{1-x}K_x)Fe_2As_2$ single crystals, it is also observed for self flux single crystals doped with nickel, cobalt, rhodium and palladium [31, 34, 41, 44]. The increase in the resistivity curve observed near ∼85 K is only observed for single crystals from the self and Sn flux method. For nickel, cobalt, rhodium and palladium doping, it was concluded that the increase in

the resistivity was caused by the spin density wave transition. But Sun *et al.*[22], Wang *et al.*[4] and Johrendt *et al.*[17] concluded that the spin density wave was absent from Sn flux $(Ba_{1-x}K_x)Fe_2As_2$ single crystals since the 140 K SDW transition is not observed. The absence of the SDW transition was attributed to the inclusion of Sn in the crystal structure. Even though Ni *et al.*[5] did not conclude that a SDW transition was present in the single crystals, the results from other literature[31, 44] implies that the increase in resistivity is due a SDW transition. Thus the increase in the resistivity curves observed for BKFA-2-Aa, BKFA-3-A and BKFA-4-A may be attributed to the SDW transition.

The presence of secondary phases in the doped single crystals was also examined using the resistivity curves. For BKFA-5-A, BKFA-2-Aa and BKFA-3-A, the resistivity curves were observed to drop to zero quickly below the superconducting transition. Due to the rapid drop in the resistivity, it was concluded that no secondary phases were present for BKFA-5-A, BKFA-2-Aa and BKFA-3-A. For BKFA-2-Ab, BKFA-4-A and BKFA-6-A, the resistivity curves were observed to slowly decrease to zero with multiple transitions. For BKFA-2-Ab, it was observed that the dominant superconducting transition occurs at 24.9 K with a secondary superconducting transition at 30.0 K. For BKFA-4-A, it was observed that the dominant superconducting transition occurs at 36.4 K with many secondary superconducting transitions occurring along the curved section of the low temperature resistivity. For BKFA-6-A, the presence of the multiple phases was observed even though a significant variation in the low temperature portion of the resistivity curve was found for single crystals from the top, middle and bottom of the crucible. It was observed that single crystal from the top of the crucible had a dominant superconducting transition at 26.7 K with a secondary superconducting transition at 15 K while single crystals from the middle of the crucible had a dominant superconducting transition at 26.2 K with many

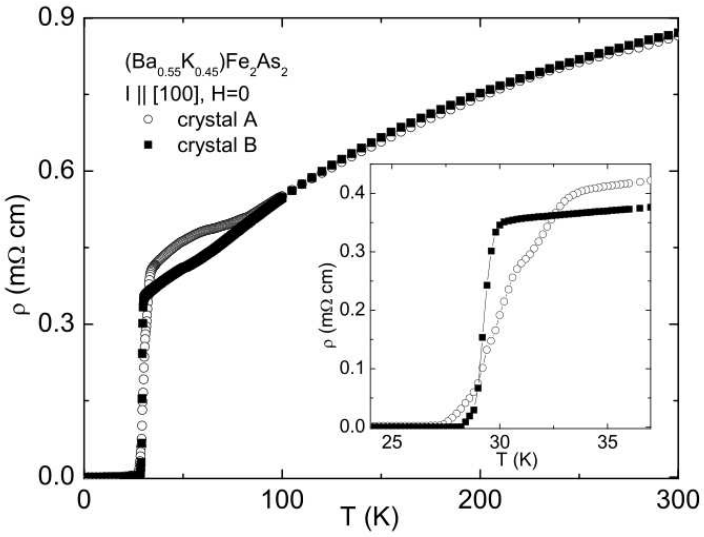

Figure 3.22: The temperature dependence of the in-plane resistivity for Sn flux single crystals of $(Ba_{0.55}K_{0.45})Fe_2As_2$. Inset: The expanded view of the superconducting transitions for the two single crystals. Reprinted from [5].

secondary superconducting transitions occurring along the curved section of the low temperature resistivity. It was observed that single crystals from the bottom of the crucible had a dominant superconducting transition at 8.7 K with a secondary superconducting phase at 5 K. It was also found that the resistivity curve for single crystal from the bottom of the crucible did not reach zero for T>5 K. Since the resistivity curve did not approach zero, it was concluded that additional non superconducting phases were also present in the single crystals. Overall, it was found that the presence of secondary phases observed using magnetic measurements and resistivity were in agreement with the exception of BKFA-5-A. For BKFA-5-A, it was found that secondary phases were present using the magnetization measurements while the resistivity measurements indicated the presence of a dominant phase only. The differing results were attributed to the variation of potassium in the single crystal growth.

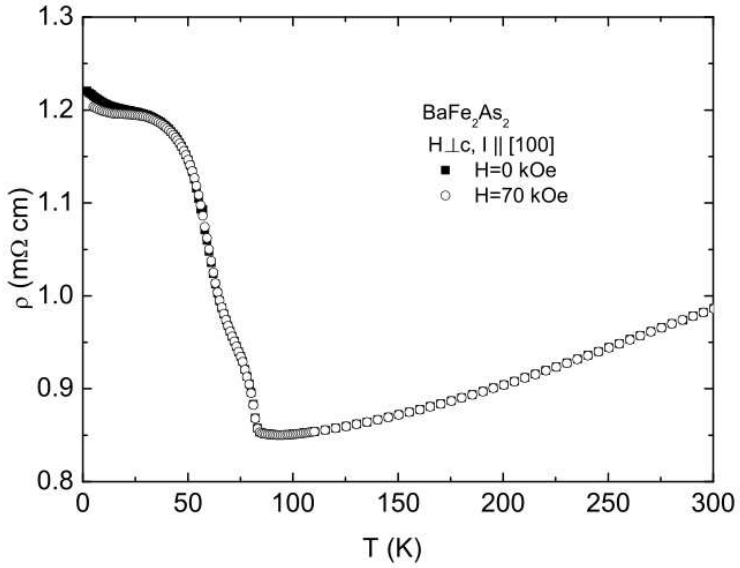

Figure 3.23: Temperature dependent in-plane resistivity for Sn flux $BaFe_2As_2$. Reprinted from [5].

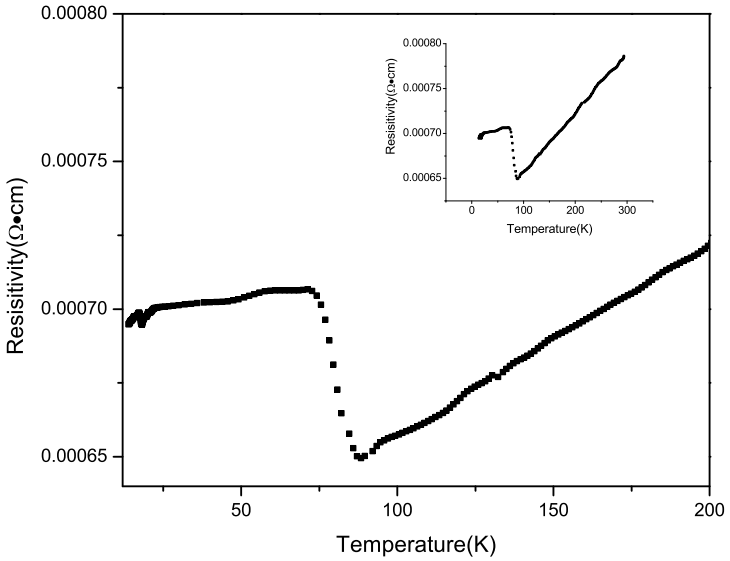

Figure 3.24: Temperature dependent in-plane resistivity for BKFA-1-NA. Inset: The temperature dependent in-plane resistivity for BKFA-1-NA up to 300 K.

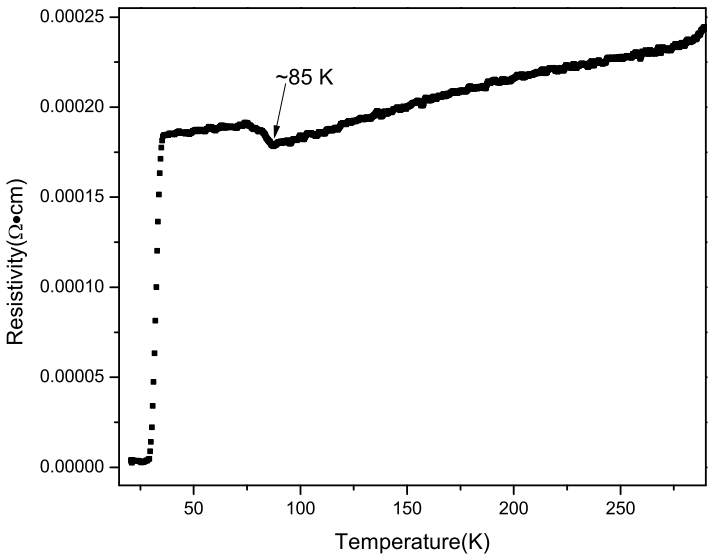

Figure 3.25: Temperature dependent in-plane resistivity for BKFA-2-Aa.

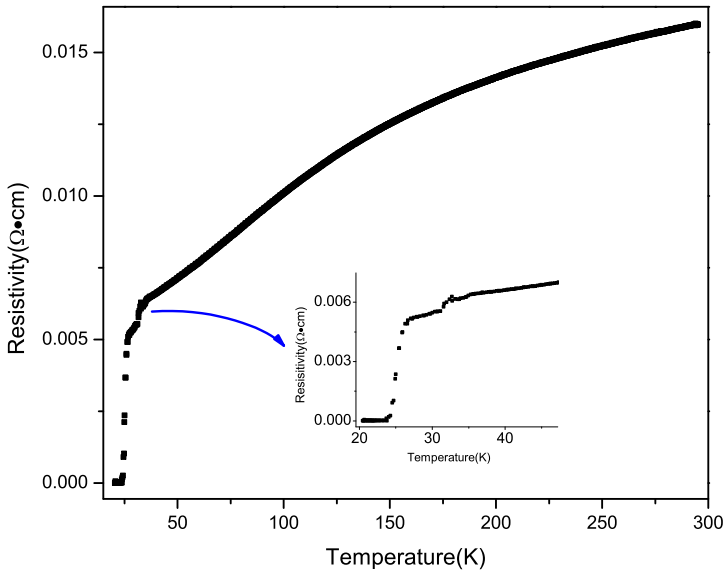

Figure 3.26: Temperature dependent in-plane resistivity for BKFA-2-Ab.

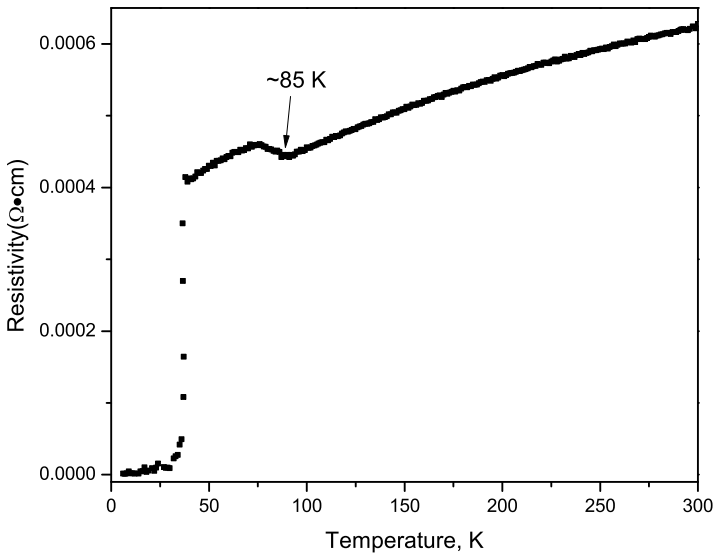

Figure 3.27: Temperature dependent in-plane resistivity for BKFA-3-A.

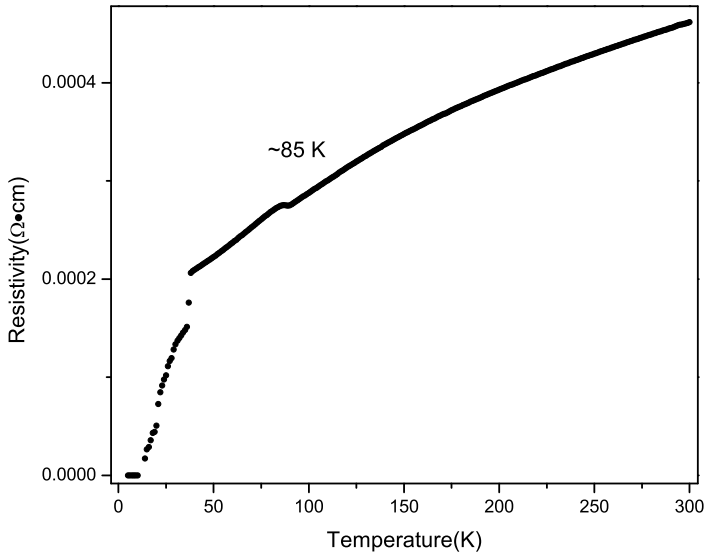

Figure 3.28: Temperature dependent in-plane resistivity for BKFA-4-A.

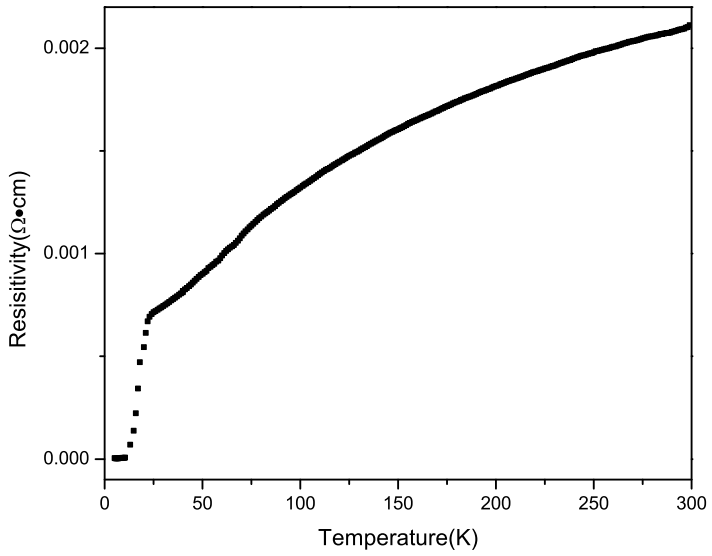

Figure 3.29: Temperature dependent in-plane resistivity for BKFA-5-A.

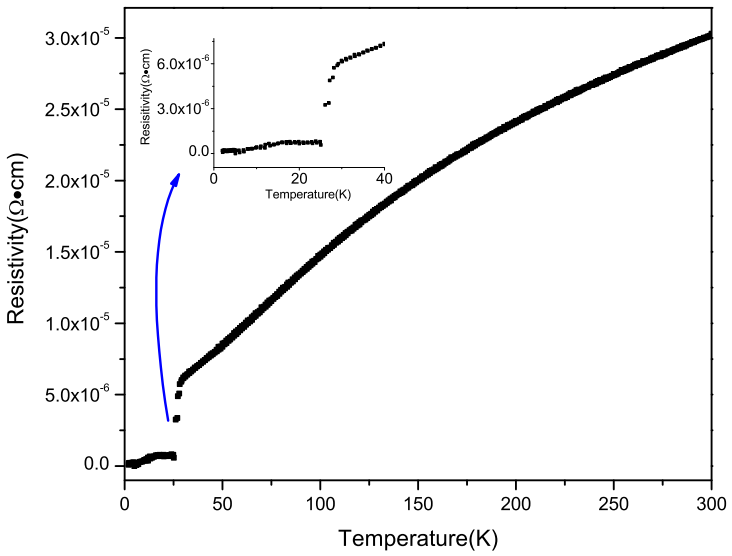

Figure 3.30: Temperature dependent in-plane resistivity for a BKFA-6-A single crystal from the top of the crucible.

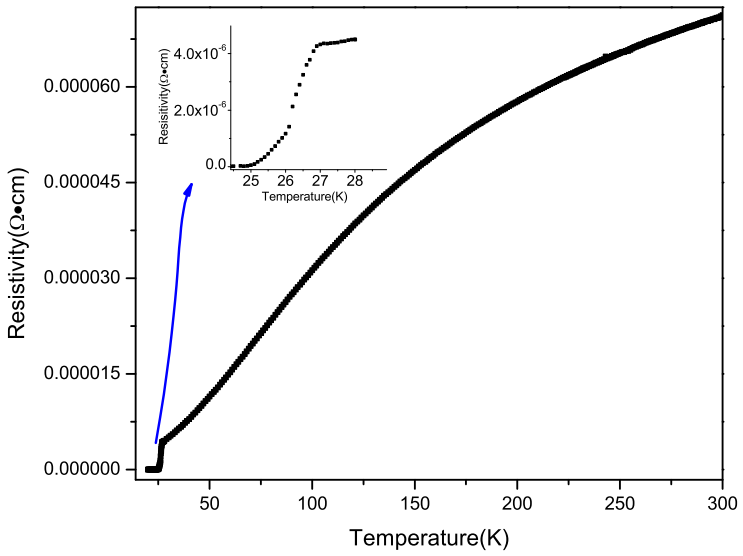

Figure 3.31: Temperature dependent in-plane resistivity for a BKFA-6-A single crystal from the middle of the crucible.

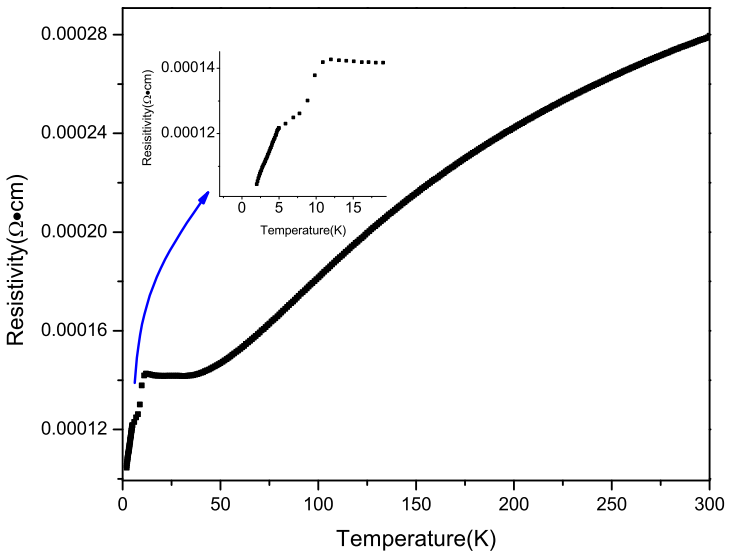

Figure 3.32: Temperature dependent in-plane resistivity for a BKFA-6-A single crystal from the bottom of the crucible.

Chapter 4

Conclusions

Single crystals of $(Ba_{1-x}K_x)Fe_2As_2$ were prepared using the Sn flux method. Six batches of single crystals were prepared using two temperature profiles: the slow heating and rapid heating methods. It was found that the single crystals grown using the slow heating method were not superconducting due to a significant loss of potassium. When the rapid heating method was used, the single crystals were observed to be superconducting with the desired potassium concentration.

The grown single crystals were first characterized using energy dispersive X-ray spectroscopy (EDS) and single crystal X-ray diffraction. The EDS analysis indicated the presence of multiple phases in the single crystals. The most interesting aspects of the EDS analysis were the presence of two distinct phases and spontaneous stoichometry changes. The two distinct phases were observed using scanning electron microscopy. Using EDS analysis, the potassium and barium concentrations were observed to be interchanged at the transition between the two phases of a single crystal. Using single crystal X-ray diffraction, the crystal structure of the single crystals was found to be I4/mmm tetragonal at room temperature. The lattice parameters of the single crystal generally agreed with the results from literature but discrepancies were still observed. The discrepancies were attributed to the variations in potassium concentration within each single crystal batch.

The magnetic properties of the single crystals were examined using temperature and field dependent magnetization measurements. The temperature dependent mag-

netization curves for the non superconducting single crystals displayed anisotropy and paramagnetic behavior. The presence of the orthorhombic distortion transition($\sim$ 85 K) was also observed for the non superconducting single crystals. The superconducting transition temperatures for the grown single crystals ranged from 8.7 K to 37.1 K. The large differences in the superconducting transition temperatures were attributed to the intentional variation in the amounts of potassium used in the growth of different batches as well as variation of potassium distribution in the individual single crystals from the same batch. The superconducting transitions in superconducting single crystals displayed a shallow slope with respect to temperature due to the presence of secondary phases. Using high field temperature dependent magnetization, the presence of the orthorhombic distortion transition was also observed for superconducting single crystals. Using field dependent magnetization measurements, the presence of magnetic impurities was detected. The magnetic impurities were caused by excess amounts of iron or iron oxide compounds in the single crystals. The effect of annealing on superconducting single crystals was studied using temperature dependent magnetization measurements. When the single crystals were annealed at 200^{o}C, the diamagnetic flux expulsion increased due to the reorganization of Ba/K in the crystal structure and the reduction of stress induced during decantation. When the single crystals were annealed again at 250^{o}C, the diamagnetic flux expulsion decreased due to a loss of potassium and variation of crystal stoichiometry.

The electrical properties of the single crystals were examined using temperature dependent resistivity measurements. The resistivity for all single crystals varied between 10^{-3} and 10^{-5} Ω·cm. The variation in the resistivity was attributed to cracks and defects in the single crystals. The resistivity curves for the non superconducting single crystals displayed metallic behavior above 85 K and semiconducting behavior below 85 K. The occurrence of weak superconducting phases was also observed

for the non superconducting single crystals. The presence of these superconducting phases was attributed to the presence of a small amount of potassium in the non superconducting single crystals. The resistivity for the superconducting single crystals increased logarithmically or linearly with increasing temperature. The logarithmic increase in the resistivity denotes the saturation of resistivity but the exact cause of the logarithmic increase was unclear. The presence of secondary phases was detected in resistivity curves for the superconducting single crystals. The superconducting single crystals also displayed an increase in resistivity with decreasing temperature around $\sim$ 85 K. The increase in the resistivity was attributed to a spin density wave transition. The spin density wave transitions were not observed using magnetic measurements. More research must be performed to determine if the SDW transition is present in Sn flux flux single crystals of $(Ba_{1-x}K_x)Fe_2As_2$.

Appendix A

Additional References

The following references are more detailed sources for certain topics:

A.1 Mössbauer Spectroscopy

G. M. Bancroft. *Mössbauer Spectroscopy: An Introduction for Inorganic Chemists and Geochemists*, **McGraw-Hill Book Company Ltd.** - London, U.K.:1973.

H. Frauenfelder. *The Mössbauer Effect*, **W. A. Benjamin, Inc.** - New York, New York: 1963.

T. C. Gibb. *Principles of Mössbauer Spectroscopy*, **Chapman and Hall Ltd.** - London: 1976.

N. N. Greenwood and and T. C. Gibb. *Mössbauer Spectroscopy*, **Chapman and Hall Ltd.** - London: 1971.

L. May. *An Introduction to Mössbauer Spectroscopy*, **Plenum Press** - New York, New York:1971.

R. V. Parish. *NMR, NQR, EPR, and Mössbauer Spectroscopy in Inorganic Chemistry*, **Ellis Horwood Ltd.** - New York, New York:1990.

A.2 Spin Density Waves

C. P. Enz. *A Course on Many-Body Theory Applied to Solid-State Physics*, **World Scientific** - Singapore: 1992.

E. Fawcett. Spin-density-wave antiferromagnetism in chromium. *Review of Modern Physics*.**60**(1):209,1988.

P. Fazekas. *Lecture Notes on Electron Correlation and Magnetism*, **World Scientific** - Singapore:1999.

G. Grüner. *Density Waves in Solids*, **Perseus Publishing** - Cambridge, Massachusetts: 1994.

W. A. Harrison. *Electronic Structure and the Properties of Solids*, **W. H. Freeman and Company** - San Francisco: 1980.

A.3 SQUID Magnetometry

J. Clarke, W. M. Goubau and M. B. Ketchen. *Tunnel Junction dc SQUID: Fabrication, Operation, and Performance*, **Journal of Low Temperature Physics, Vol. 25, Issue 1** - New York, New York: 1976.

J. C. Gallop. *SQUIDs, the Josephson Effects and Superconducting Electronics*, **Adam Hilger** - New York, New York: 1990.

M. McElfresh. *Fundamentals of Magnetism and Magnetic Measurements featuring QD's MPMS system*, **http://www.qdusa.com/resources/techdocs.html**: 1994.

M. McElfresh, S. Li and R. Sager. *Effects of Magnetic Field Uniformity on the Measurement of Superconducting Samples*, **http://www.qdusa.com/resources/techdocs.html**

S. T. Ruggiero and D. A. Rudman. *Superconducting Devices*, **Academic Press, Inc.** - New York, New York: 1990.

M. Tinkham. *Introduction to Superconductivity*, **McGraw-Hill Inc.** - Toronto, Canada: 1996.

Bibliography

[1] Y. Kamihara, T. Watenabe, M. Hirano, and H. Hosono. Iron-Based Layered Superconductors La[$O_{1-x}F_x$]FeAs (x = 0.05 – 0.12) with T_c = 26 K. *J. Am. Chem. Soc.*, 130:3296 – 3297, 2008.

[2] H. Takahashi, K. Igawa, K. Arii, Y. Kamihara, M. Hirano, and H. Hosono. Superconductivity at 43 K in a iron-based layered compound $LaO_{1-x}F_xFeAs$. *Nature*, 453(376 - 378), 2008.

[3] M. Rotter, M. Tegel, and D. Johrendt. Superconductivity at 38 K in the Iron Arsenide $(Ba_{1-x}K_x)Fe_2As_2$. *Phys. Rev. Lett.*, 101(107006), 2008.

[4] X. F. Wang, T. Wu, G. Wu, H. Chen, Y. L. Xie, J. J. Ying, Y. J. Yan, R. H. Liu, and X. H. Chen. Growth and Anisotropy in transport properties and susceptibility of single crystals $BaFe_2As_2$. *Phys. Rev. Lett.*, 102(117005), 2009.

[5] N. Ni, S. L. Bud'ko, A. Kreyssig, S. Nandi, G. E. Rustan, A. I. Goldman, S. Gupta, J. D. Corbett, A. Kracher, and P. C. Canfield. Anisotropic thermodynamic and transport properties of single crystalline $(Ba_{1-x}K_x)Fe_2As_2$ (x=0 and 0.45). *Phys. Rev. B*, 78(014507), 2008.

[6] Anupam, P. L. Paulose, H. S. Jeevan, C. Geibel, and Z. Hossain. Interplay between superconductivity and magnetism in K-doped $EuFe_2As_2$. *Prog. Theor. Phys.*, 121:915, 2009.

[7] F. Ronning, T. Klimczuk, E. D. Bauer, H. Volz, and J. D. Thompson. Systhesis and properties of $CaFe_2As_2$ single crystals. *J. Phys.:Condens. Matter*, 20 (322201), 2008.

[8] K. Sasmal, B. Lv, B. Lorenz, A. M. Guloy, F. Chen, Y. Y. Xue, and C. W. Chu. Superconductivity up to 37 K in $(A_{1-x}Sr_x)Fe_2As_2$ with A = K and Cs. *Phys. Rev. Lett.*, 101(107007), 2008.

[9] X. C. Wang, Q. Q. Liu, Y. X. Lv, W. B. Gao, L. X. Yang, R. C. Yu, F. Y. Li, and C. Q. Jin. The superconductivity at 18 K in LiFeAs system. *Solid State Comm.*, 148:538–540, 2008.

[10] M. J. Pitcher, D. R. Parker, P. Adamson, S. J. C. Herkelrath, A. T. Boothroyd, R. M. Ibberson, M. Brunelli, and S. J. Clarke. Structure and superconductivity of LiFeAs. *Chem. Commun.*, 45:5918–5920, 2008.

[11] J. H. Tapp, Z. Tang, B. Lv, K. Sasmal, B. Lorenz, P. C. W. Chu, and A. M. Guloy. LiFeAs:An intrinsic FeAs-based superconductor with T_c = 18 K. *Phys. Rev. B*, 78(060505), 2008.

[12] S. Matusishi, Y. Inoue, T. Nomura, M. Hirano, and H. Hosono. Cobalt-Substitution-Induced Superconductivity in a New Compound with ZrCuSiAs-Type Structure, SrFeAsF. *J. Phys. Soc. Jpn.*, 77(113709), 2008.

[13] F. Han, X. Zhu, G. Mu, P. Cheng, and H. H. Wen. SrFeAsF as a parent compound for iron pnictide superconductors. *Phys. Rev. B*, 78(180503), 2008.

[14] Y. Kamihara, H. Hiramatsu, M. Hirano, R. Kawamura, H. Yanagi, T. Kamiya, and H. Hosono. Iron-Based Layered Superconductor: LaOFeP. *J. Am. Chem. Soc.*, 128:10012–10013, 2006.

[15] Z. A. Ren, W. Lu, J. Yang, X. L. Shen, Z. C. Li, G. C. Che, X. L. Dong, L. L. Sun, F. Zhou, and Z. X. Zhao. Superconductivity at 55 K in Iron-Based F-Doped Layered Quaternary Compounds $Sm[O_{1-x}F_x]FeAs$. *Chin. Phys. Lett.*, 25 (6):2215, 2008.

[16] D. Johrendt and R. Pöttgen. Pnictide Oxides: A New Class of High-T_c Superconductors. *Angew. Chem. Int. Ed.*, 47:4782–4784, 2008.

[17] D. Johrendt and R. Pöttgen. Superconductivity, magnetism and crystal chemistry of $Ba_{1-x}K_xFe_2As_2$. *arXiv:cond-mat/0902.1085*, 2009.

[18] M. Rotter, M. Tegel, D. Johrendt, I. Schellenberg, W. Hermes, and R. Pöttgen. Spin-density-wave anomaly at 140 K in ternary iron arsenide $BaFe_2As_2$. *Phys. Rev. B*, 78(020503), 2008.

[19] Y. Y. Sun, I. Rusakova, R. L. Meng, Y. Cao, P. Gautier-Picard, and C. W. Chu. The 23 K superconducting phase YPd_2B_2C. *Physica C*, 230(3-4):435–442, 1994.

[20] G. Wu, R. H. Liu, H. Chen, Y. J. Yan, Y. L. Xie, J. J. Ying, X. F. Wang, D. F. Fang, and X. H. Chen. Transport properties and superconductivity in $Ba_{1-x}M_xFe_2As_2$ (M=La and K) with double FeAs layers. *Europhys. Lett.*, 84: 27010, 2008.

[21] M. Rotter, M. Pangerl, M. Tegel, and D. Johrendt. Superconductivity and Crystal Structures of $(Ba_{1-x}K_x)Fe_2As_2$(x=0-1). *Angew. Chem. Int. Ed.*, 47(41):7949–7952, 2008.

[22] G. L. Sun, D. L. Sun, M. Konuma, P. Popovich, A. Boris, J. B. Peng, K. Y. Choi, P. Lemmens, and C. T. Lin. Iron pnictides: Single crystal growth and

effect of doping on structural transport and magnetic properties. *arXiv:cond-mat/0901.2728*, 2009.

[23] Y. Su, P. Link, A. Schneidewind, T. Wolf, P. Adelmann, Y. Xiao, M. Meven, R. Mattal, M. Rotter, D. Johrendt, T. Brueckel, and M. Loewenhaupt. Neutron Diffraction on antiferromagnetic ordering in single-crystal $BaFe_2As_2$. *Phys. Rev. B*, 79(064504), 2009.

[24] C. de la Cruz, Q. Huang, J. W. Lynn, J. Li, W. Ratcliff II, J. L. Zarestky, H. A. Mook, G. F. Chen, J. L. Luo, N. L. Wang, and P. Dai. Magnetic Order close to superconductivity in the iron-based layered $LaO_{1-x}F_xFeAs$ system. *Nature*, 453:899 – 902, 2008.

[25] J. Dong, H. J. Zhang, G. Xu, Z. Li, G. Li, W. Z. Hu, D. Wu, G. F. Chen, X. Dai, J. L. Luo, Z. Fang, and N. L. Wang. Competing Orders and Spin-Density-Wave Instability in $La(O_{1-x}F_x)FeAs$. *Europhys. Lett.*, 83:27006, 2008.

[26] Q. Huang, Y. Qiu, Wei bao, J. W. Lynn, M. A. Green, Y. Chen, T. Wu, G. Wu, and X. H. Chen. Magnetic order in $BaFe_2As_2$, the parent compound of the FeAs based superconductors in a new structural family. *Phys. Rev. Lett.*, 101:257003, 2008.

[27] S. D. Wilson, Z. Yamani, C. R. Rotundu, B. Freelon, E. Bourret-Courchesne, and R. J. Birgeneau. The nature of the magnetic and structural phase transitions in $BaFe_2As_2$. *Phys. Rev. B*, 79:184519, 2009.

[28] S. Jiang, C. Wang, Z. Ren, Y. Luo, G. Cao, and Z. Xu. Superconductivity in $BaFe_2(As_{1-x}P_x)_2$. *arXiv:cond-mat/0901.3227v1*, 2009.

[29] P. L. Alireza, Y. T. C. Ko, J. Gillett, C. M. Petrone, J. M. Cole, S. E. Sebastian, and G. G. Lonzarich. Superconductivity up to 29 K in $SrFe_2As_2$ and $BaFe_2As_2$ at high pressure. *J. Phys.:Condens. Matter*, 21(1):012208, 2008.

[30] H. Fukazawa, N. Takeshita, T. Yamazaki, K. Kondo, K. Hirayama, Y. Kohori, K. Miyazawa, H. Kito, H. Eisaki, and A. Iyo. Suppression of magnetic order by pressure in $BaFe_2As_2$. *J. Phys. Soc. Jpn.*, 77:105004, 2008.

[31] L. J. Liu, Q. B. Wang, Y. K. Luo, H. Chen, Q. Tao, Y. K. Li, X. Lin, M. He, Z. W. Zhu, G. H. Cao, and Z. A. Xu. Superconductivity induced by Ni doping in $BaFe_2As_2$. *New J. Phys.*, 11:025008, 2009.

[32] M. A. Tanatar, N. Ni, C. Martin, R. T. Gordon, H. Kim, V. G. Kogan, G. D. Samolyuk, S. L. Bud'ko, P. C. Canfield, and R. Prozorov. Anisotropic of the Optimally-Doped Iron Pnictide Superconductor $Ba(Fe_{0.926}Co_{0.074})_2As_2$. *Phys. Rev. B*, 79:094507, 2009.

[33] S. Paulraj, S. Sharma, A. Bharathi, A. T. Satya, S. Chandra, Y. Hariharan, and C. S. Sundar. Superconductivity in Ru substituted $BaFe_{2-x}Ru_xAs_2$. *arXiv:cond-mat/0902.2728*, 2009.

[34] N. Ni, A. Thaler, A. Kracher, S. L. Bud'ko, and P. C. Canfield. Phase diagrams of $Ba(Fe_{1-x}TM_x)_2As_2$. *Phys. Rev. B*, 80:024511, 2009.

[35] L. May, editor. *An Introuduction to Mössbauer Spectroscopy.* Plenum Press, 1971.

[36] R. V. Parish. *NMR, NQR, EPR, and Mössbauer Spectroscopy in Inorganic Chemistry.* Ellis Horwood, 1990.

[37] G. M. Bancroft. *Mössbauer Spectroscopy: An Introduction for Inorganic Chemists and Geochemists*. Mc-Graw Hill Book Company, 1973.

[38] M.S. Torikachvili, S. L. Bud'ko, N. Ni, and P. C. Canfield. Hydrostatic pressure study of the structural phase transitions and superconductivity in single crystals of $(Ba_{1-x}K_x)Fe_2As_2$ ($x = 0$ and 0.45) and $CaFe_2As_2$. *arXiv:cond-mat/0810.0241*, 2008.

[39] C. F. Miclea, N. Nicklas, H. S. Jeevan, D. Kasinathan, Z. Hossain, H. Rosner, P. Gegenwart, C. Geibel, and F. Steglich. Possible re-entrant superconductivity in $EuFe_2As_2$ under pressure. *Phys. Rev. B*, 79:212509, 2009.

[40] M. S. Torikachvili, S. L. Bud'ko, N. Ni, and P. C. Canfield. Effect of pressure on the structural phase transition and superconductivity in $(Ba_{1-x}K_x)Fe_2As_2$(x = 0 and 0.45) and $SrFe_2As_2$ single crystals. *Phys. Rev. B*, 78(104527), 2008.

[41] K. Ahilan, J. Balasubramaniam, F. L. Ning, T. Imai, A. S. Sefat, R. Jin, M. A. McGuire, B. C. Sales, and D. Mandrus. Pressure effects on the electrons-doped high T_c superconductors $BaFe_{2-x}Co_xAs_2$. *J. Phys.:Condens. Matter*, 20:472201, 2008.

[42] M. Gooch, B. Lv, B. Lorenz, A. M. Guloy, and C. W. Chu. Pressure effects on the superconducting and spin-density wave transitions in the phase diagram of $K_{1-x}Sr_xFe_2As_2$. *Phys. Rev. B*, 78:180508, 2008.

[43] H. Q. Yuan, J. Singleton, F. F. Balakirev, S. A. Baily, G. F. Chen, J. L. Luo, and N. L. Wang. Nearly isotropic superconductivity in (Ba,K)Fe_2As_2. *Nature*, 457:565 – 567, 2009.

[44] F. Ning, K. Ahilan, T. Imai, A. S. Sefat, R. Jin, M. A. McGuire, B. C. Sales, and D. Mandrus. Spin Susceptibility, Phase Diagram, and Quantum Criticality in the Electron-Doped High T_c Superconductor $Ba(Fe_{1-x}Co_x)_2As_2$. *J. Phys. Soc. Jpn.*, 78:013711, 2009.

[45] P. Reuvekamp, F. S. Razavi, C. Hoch, J. S. Kim, R. K. Kremer, and A. Simon. Spontaneous Stoichiometry Change in Single Crystals of Superconducting $(Ba_{1-x}K_x)Fe_2As_2$ Grown by a Rapid-Heating Sn-Flux Method. *J. Supercond. Nov. Magn.*, 22:353–356, 2009.

[46] M. G. Kanatzidis, R. Pöttgen, and W. Jeitschko. The Metal Flux: A Preparative Tool for the Exploration of Intermetallic Compounds. *Angew. Chem. Int. Ed.*, 44(6996-7023), 2005.

[47] P. Jolibois and C. R. Hebd. *Seances Acad. Sci.*, 150(106-108), 1910.

[48] P. C. Canfield and Z. Fisk. Growth of single crystals from metallic fluxes. *Phil. Mag. B.*, 65(6):1117–1123, 1992.

[49] T. Motohashi, E. Naujalis, R. Ueda, K. Isawa, M. Karppinen, and H. Yamauchi. Simultaneously enhanced thermoelectric power and reduced resistivity of $Na_xCo_2O_4$ by controlling Na nonstiochiometry. *Appl. Phys. Lett.*, 79(10): 1480–1482, 2001.

[50] G. H. Stout and L. H. Jensen. *X-ray Structure Determination.* Macmillian Publishing Co. Inc., 1968.

[51] M. Rotter, M. Tegel, I. Schellenberg, F. M. Schappacher, R. Pöttgen, J. Deisenhofer, A. Günther, F. Schrettle, A. Loidl, and D. Johrendt. Competition of mag-

netism and superconductivity in underdoped $(Ba_{1-x}K_x)Fe_2As_2$. *New J. Phys.*, 11(025014), 2009.

[52] D. Jiles. *Introduction to Magnetism and Magnetic Materials*. Chapman and Hall, 1991.

[53] L. J. van der Pauw. A method of measuring the resistivity and hall coefficient of lamellae of arbitary shape. *Philips Techinical Review*, 20:220 – 224, 1958.

[54] O. Gunnarsson, M. Calandra, and J. E. Han. Colloquium: Saturation of electrical resistivity. *Review of Modern Physics*, 75:1085–1099, 2003.